High-Power Antenna Feed Based on Spatial Power Combining Technology

Phase 1

Nicolas Gagnon, Aldo Petosa and John Bradley
CRC Report No. CRC-RP-2007-001
Ottawa, Ontario

May 2006

Canada

CRC

High-Power Antenna Feed Based on Spatial Power Combining Technology

Phase 1

Nicolas Gagnon, Aldo Petosa and John Bradley

CRC Report No. CRC-RP-2007-001

Ottawa, Ontario

Canada

CRC

High-Power Antenna Feed Based on Spatial Power Combining Technology
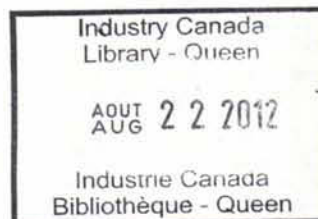
Phase 1

Nicolas Gagnon, Aldo Petosa and John Bradley

CRC Report No. CRC-RP-2007-001

Ottawa, May 2006

CAUTION
This information is provided with
the express understanding that
proprietary and patent rights will
be protected

<This page intentionally left blank>

Abstract

This document describes the first phase of the design of two spatial power combiners having a high output power. These spatial power combiners were chosen as candidates for feeding a reflectarray antenna. This antenna is intended to be used as part of the uplink for wideband multimedia satellite systems operating in the Ka band.

The first design was a multilayer reflective tile composed of 37 elements. The first step of the process involved the design of a passive single element antenna on a thin ground plane. Good measurement results were obtained for both return loss and radiation patterns. Next, a passive single element on thick substrate was designed and fabricated. A thick ground plane was used for heat dissipation purposes and for mechanical rigidity, which would be necessary in the active version of the array. Again good measurement results were obtained. Then, a passive 37-element spatial power combining reflectarray was fabricated. Results revealed an acceptable amplitude profile for the illumination of the main reflectarray. In the final design step, a 4-element active reflectarray was built and measured as a proof of concept.

The second design was a transmissive tray composed of 36 elements. The single element antenna was perpendicularly fed through an aperture in the ground plane. A single element prototype was built and measured. The measurement results obtained were good and had a fair agreement with the simulation results. The small discrepancy between measurement and simulation was caused by an undesired gap at the junction of the antenna and feed substrates in the fabricated structure.

Résumé

Ce document présente la première phase de la conception de deux configurations de combinaison spatiale de puissance ayant une puissance de sortie élevée. Ces deux configurations ont été choisies pour alimenter une antenne de type réseau réflecteur. L'antenne a été conçue pour être utilisée en liaison montante pour les systèmes de satellite multimédia à large bande opérant dans la bande Ka.

La première configuration consistait en un montage en mosaïque (« tile ») de type réfléchissant composé de 37 éléments. L'antenne passive constituant un élément simple a initialement été développée et fabriquée sur un plan de masse mince. Les résultats expérimentaux obtenus pour le coefficient de réflexion et les diagrammes de rayonnement étaient bons dans les deux cas. Une antenne passive à élément simple sur un plan de masse épais a ensuite été conçue et fabriquée. Le plan de masse épais a servi à améliorer la dissipation thermique et la rigidité de la structure, lesquelles seront nécessaires lors de la conception de la version active du réseau. Encore une fois, de bons résultats expérimentaux ont été obtenus. Une version passive du réseau réflecteur utilisé pour la combinaison spatiale de puissance et composé de 37 éléments fut fabriquée ultérieurement. Les résultats ont démontré un profil d'amplitude acceptable pour l'illumination du réseau réflecteur principal. Finalement, une version active du réseau réflecteur servant à la combinaison spatiale de puissance et composée de quatre éléments fut construite et mesurée dans le but de démontrer le concept.

La deuxième configuration consiste en un montage en plateaux parallèles (« tray ») composé de 36 éléments. L'antenne était alimentée de façon perpendiculaire au moyen d'une fente dans le plan de masse. Un élément simple a été construit et mesuré. Les résultats de mesure obtenus étaient acceptables et relativement en accord avec les résultats de simulation. Les résultats mesurés et simulés divergeaient légèrement en raison d'un espacement non désiré à la jonction du substrat de l'alimentation et du substrat de l'antenne sur la structure fabriquée.

Table of Contents

List of Figures

List of Tables

1. Introduction [1]

With the licensing of the Multimedia Satellite band in North America, it is foreseen that fixed and mobile Ka-band dual-link terminals will be commercialised in the upcoming years. These communications links between the Earth and satellites require high effective isotropic radiated power (EIRP). Since these terminals are preferred to be portable and/or compact, the antenna size is usually relatively small and, to maintain a high EIRP, high output power is required. For uplink communications, solid-state high-power amplifiers are attractive for their low cost, light weight, compactness and ease of integration to microstrip technology.

At low microwave frequencies, the output power of high-power MMIC amplifiers is higher than 10 W. At Ka band and higher, the output power of MMIC amplifiers is typically less than 4 W. Furthermore, corporate feed networks at Ka band and millimetre waves are not practical because of high metal and substrate losses. Additionally, efficient power dividers/combiners are not possible due to high power leakage [2]. Therefore, other ways are needed to combine the available output power from each device in order to obtain higher total output power.

Spatial power combining, which consists of transmitting a signal into free-space and amplifying it spatially with an active array, was first introduced as an alternative to circuit combining in the mid-1980's. It is the subject of numerous studies since the mid-1990's. Unlike corporate feed networks, spatial power combiners do not suffer from high power leakage and they are well suited to high output power applications.

In order to meet the high output power requirement of an uplink satellite communications system at Ka band, spatial power combining technology was used. The present document reports on the first phase of the design of a feed for a reflectarray based on spatial power combining technology.

This report is divided as follows: first, a short theoretical background as well as a brief survey of existing technologies are presented; next, a description of the design project is provided, in which different spatial power combining configurations are presented; then, a reflective mutilayer tile and a transmissive tray, which were chosen as potential candidates for the current application, are described in details; finally, conclusions are made and details on potential future work to be performed are reported.

1

1.1. Theoretical Background

1.1.1. Power Combining

In some high-frequency communications applications, usually ones involving transmissions between Earth and satellite, high output power is required. At Ka band and higher frequencies, it is difficult to obtain the necessary power from MMIC devices due to their limited output power (typically lower than 4 W). Furthermore, as the maximum output power of an amplifier increases, the size of the MMIC chip also increases. Therefore, some ways are needed to combine the available output power from each device in order to obtain higher output power.

Traditionally, the combining is performed in microstrip technology using a corporate feed network, as shown in Figure 1(a). While this is efficient at microwave frequencies, it is not a very attractive solution for achieving high output power at millimetre waves due to the presence of high conductor and substrate losses for the transmission lines and also because efficient power dividers/combiners are not possible due to high power leakage. In fact, it can be shown [2] that the output power from a circuit-based corporate feed network reaches its peak for an optimum number of amplifiers, and using more amplifiers actually results in a lower output power value. This is depicted in Figure 2.

An alternative to the corporate feed network is a quasi-optical combining technique, as shown in Figure 1(b). Usually called spatial combining in non quasi-optical applications (i.e. applications not involving Gaussian beams, such as antenna arrays), this technology uses free-space (rather than transmission lines) as a transmission medium to propagate the signal and then amplify it. The term spatial power combining usually refers to using this technology to obtain high output power.

Spatial power combining is attractive when many amplifiers are used and a high output power is required. It also offers a better noise figure since, in theory, the noise figure of the whole configuration is the same as the noise figure of a single element, as well as a graceful degradation. However, it is difficult to model and there is always a trade-off between spillover losses and amplitude/phase uniformity. This can be explained as follows: if the beam incident on the amplifier array is narrow, most of the incident power will be captured by the array thus the spillover efficiency will be high. However, many amplifiers of the spatial power combining array will be far from the saturated power, resulting in a lower total output power. On the other hand, for a wider beam, the amplitude distribution across the amplifier array will be more uniform, so that all amplifiers will be near their maximum output power. The output power is therefore potentially maximised; however, the array will not be able to capture all of the incident power, which corresponds to a spillover efficiency drop. In addition, the wider beam implies a feed antenna with a lower gain, so that the

2

AMPLIFIER

INPUT

(a)

INPUT
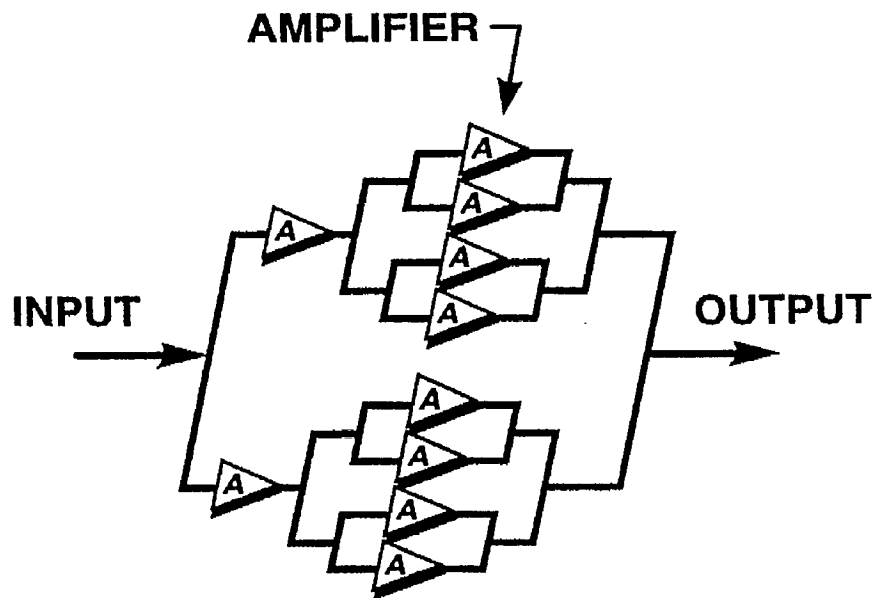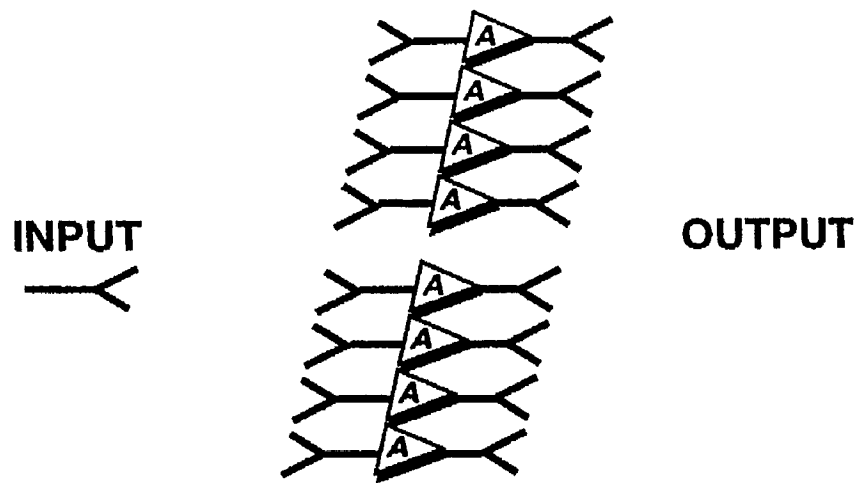
(b)

Figure 1: Combining technologies (a) Corporate feed network (circuit combining); (b) Spatial (power) combining (from [3]).

3
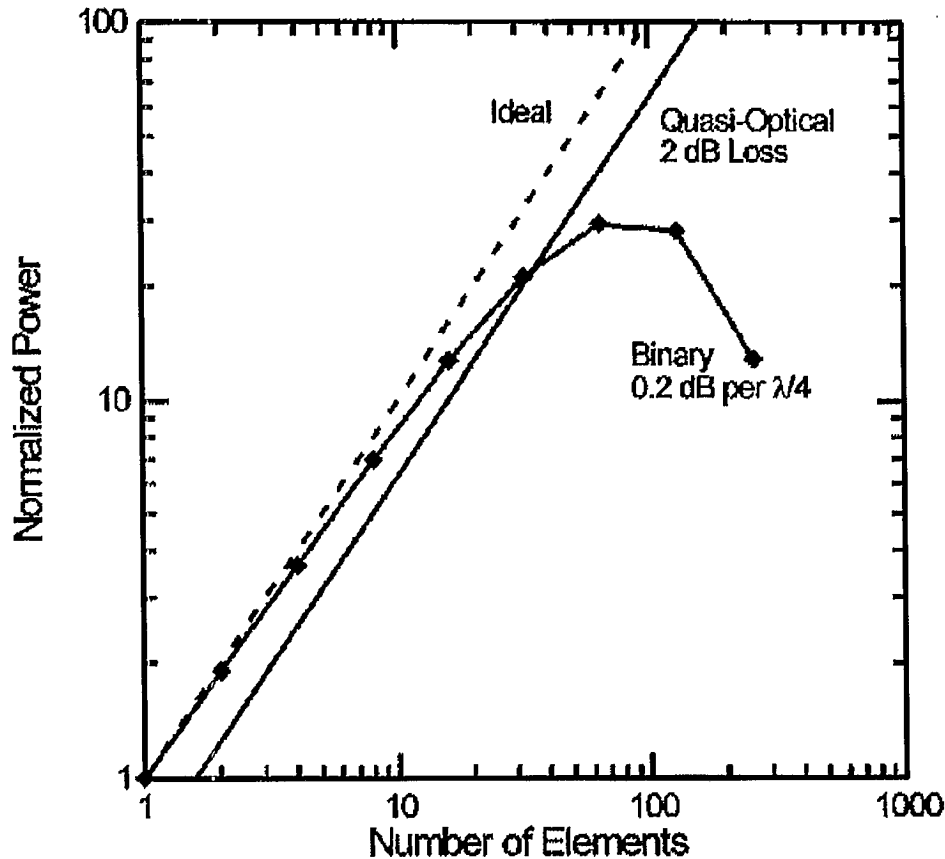
Figure 2: Output power from a binary combiner (see Figure 1(a)) and from a quasi-optical combiner (see Figure 1(b)) at Ka band (from [2]).

incident power on the array is lower, and thus more amplification is required. However, this problem can be addressed by using additional components such as lenses, which will, in counterpart, make the overall system more complex, more expensive and bulkier.

1.1.2. Spatial Power Combining Architectures

The spatial power combining structures reported can be classified as either tile or tray. The tile is the most straightforward architecture and it is an evolution of the antenna array, as shown in Figure 3(a). It is normally a multilayer structure, and is fabricated by bonding sheets of metallised substrate together. The result is a relatively flat structure, in which the input and output antennas can be easily designed with orthogonal polarisation to improve the isolation between the input and output signals in order to avoid unwanted spurious oscillation. However, the MMIC amplifiers are located on the same layer as the radiating elements, which in order to accommodate the amplifiers, must be spaced further apart. Moreover, in such a configuration, it is much more of a challenge to dissipate heat, which is necessary in high output

4
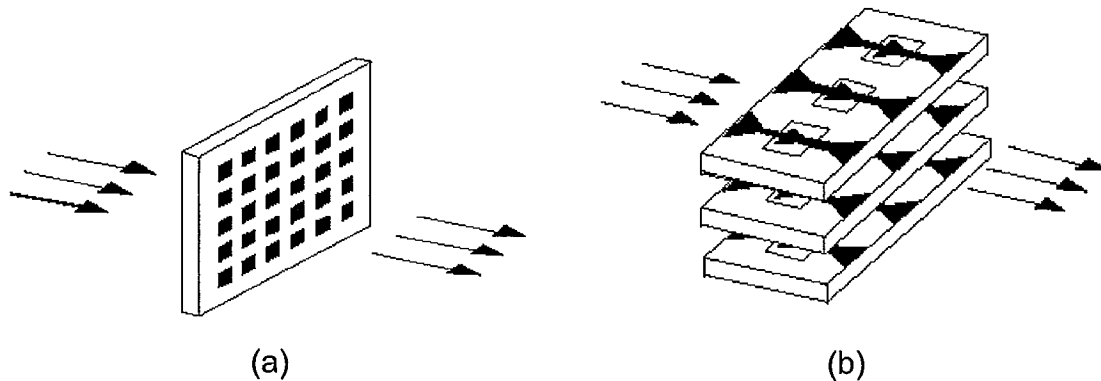
Figure 3: Spatial power combining architectures (a) Tile; (b) Tray (from [2]).

power applications. Another tile architecture, which is not composed of a traditional active array, is the grid amplifier. For further information on grid amplifiers, see [2].

The tray architecture consists of an arrangement of stacked substrate layers parallel to the direction of propagation, as shown in Figure 3(b). The radiating elements are usually end-fire elements; however it is possible to feed an array of broadside elements due to space constraints. The tray architecture allows for smaller separation between the radiating elements since the amplifiers are not located in the same plane as the radiating elements. Furthermore, the amplifiers do not interfere with the radiating elements. Dissipation of heat can be achieved more successfully with such a configuration. One of the main concerns about the tray architecture is the isolation between the receiving and transmitting elements: the isolation cannot be easily improved by using orthogonal polarisation since such a technique is difficult to implement in tray architecture. Also, the fact that this structure is thick compared to the tile makes it unsuitable for some applications. Furthermore, the mechanical requirements are much more difficult to achieve: a simple example is that, for the case of perpendicularly-fed broadside elements, perpendicular substrate layers cannot be aligned with the same precision as parallel (bounded) substrate layers, commonly used in the tile architecture, for which the technology is more mature.

1.1.3. Figures of Merit

In order to evaluate the performance of a given spatial power combining structure, some figures of merit were proposed [4]. In this section, only the major figures of merit are reported.

The most important parameter of a spatial power combiner is the output power, P_{out}, since the basic idea in using such a technology is to obtain high output power. The input power, P_{in}, is another important parameter that is used

to calculate some figures of merit. A common figure of merit is the gain of the system, G_{sys}, which relates the input power and the output power:

$$G_{sys} = \frac{P_{out}}{P_{in}}. \tag{1}$$

The input power is also used to calculate the power-added efficiency, PAE, which is a measure of how efficiently the DC power is used to amplify the RF signal:

$$PAE = \frac{P_{out} - P_{in}}{P_{DC}}. \tag{2}$$

In (2), P_{DC} is the power required to bias the devices. Finally, the last figure of merit to be presented is the combining efficiency, η_{comb}:

$$\eta_{comb} = \frac{P_{out}}{\sum_{n=1}^{N} P_{n,available}}, \tag{3}$$

where $P_{n,available}$ is the output power available from the nth amplifier and the total number of amplifiers is N. If the available output power is the same for each amplifier, then (3) reduces to

$$\eta_{comb} = \frac{P_{out}}{P_{amp} N}, \tag{4}$$

where P_{amp} is the available output power for each device. The combining efficiency determines how efficiently the power from the different amplifiers is combined.

1.2. Existing Technologies

In order to provide a comparison between the configurations that will be presented in the next chapter and the reported ones, Table I presents some existing technologies and their specifications. Only technologies developed at Ka band are reported in this table. This allows for a fair comparison between output power, device size and possible technologies. For further information on other technologies and applications at different frequency bands, see [2], [11] and [12].

6

Table I: Some existing spatial power combining technologies at Ka band.

Name	Waveguide-Fed Grid Amplifier	Quasi-Optical Amplifier Array	Perpendi-cularly-Fed Patch Array	Slotted-Wave-guide Power-Combining Circuit
Architecture	Tile	Tile	Tray	Tray
Configuration	Grid amplifier	Planar lens amplifier	Planar lens amplifier	Waveguide-based
Dimensions (mm)	10 X 10	68.6 X 53.1	N/A	N/A
Number of elements	512	45	49	8
Radiating device	Printed dipoles	Patch antennas	Patch antennas	Slots in waveguide
Frequency	34 GHz	34 GHz	31.9 GHz	33 GHz
Effective output power	5 W	25 W	5 W	1.45 W
Effective system gain	5.5 dB	10 dB	11.6 dB	17 dB
PAE (%)	21	3	N/A	13.7
Combining efficiency (%)	79	28	36	72
References	[5], [6]	[7], [8]	[9]	[10]

<This page intentionally left blank>

8

2. Project Description

2.1. Motivations

The Advanced Antenna Technology (RAAT) group was involved in the Rural and Remote Broadband Access (RRBA) research program by contributing to various projects. One of these projects was to develop a user terminal for a satellite communications link at EHF. This satellite link was designed for use in the multimedia satellite band, i.e. the 19.7-20.2 GHz band for the downlink and the 29.5-30.0 GHz band for the uplink.

The development of the uplink portion of the device was the biggest challenge at this point. The main reason was because high output power was needed, which was difficult to achieve at this frequency range. Therefore, spatial power combining technology was used in order to achieve required power output. Compared to other technologies, spatial power combining technology offered a more compact and more DC efficient solution while offering better noise figure and graceful degradation. The spatial power combining device would then be integrated in a reflector antenna as a feed for the main reflectarray.

2.2. Requirements

The major requirement about the spatial power combiner was the output power. The required output power was about 15-20 W, depending on the size and the efficiency of the reflectarray used for the terminal. The frequency of operation was from 29.5 GHz to 30 GHz, therefore the resonance frequency of the antenna elements should be about 29.75 GHz with a bandwidth of 500 MHz.

2.3. Configurations

The choice of the spatial power combining configuration depended on the application in which it would be used. In this case, the application was to feed a reflectarray. Many different factors had to be considered:

- The physical size of the spatial power combiner was a concern since the blockage must be limited;

- The spacing between the antenna elements of the spatial power combiner had to be kept as small as possible in order to increase the beam width and allow beam shaping;

- The number of elements had to be as small as possible to prevent a too narrow beam, which would result in an inefficient illumination of the reflectarray.

These factors had to be kept in consideration while choosing the candidate configurations.

2.3.1. Reflective and Transmissive Approach

For feeding the reflectarray, two approaches could be adopted:

- Directly feeding the reflectarray;

- Using a subreflecting structure to feed the reflectarray, such as the case in Cassegrain dual-reflectors.

The traditional spatial power combining arrangement is of the transmissive type, where the power from the feeding element is received on one side and transmitted on the other. If the reflectarray is directly fed, then a transmissive approach must be used. However, the spatial power combiner can also be used as a reflective structure, where the power is received on one side and transmitted on the same side. This is the case if a subreflecting array is used as a spatial power combining device. These two configurations are shown in Figure 4. In this figure, the following parameters are introduced:

- D is the diameter of the reflectarray or main reflector;

- L is the length of the reflectarray, including the feeding system;

- R is the separation between the feed horn and the spatial power combining structure;

- V_S is the diameter of the subreflecting spatial power combining surface.

In Figure 4, a tile architecture is shown for the reflective approach and a tray architecture is shown for the transmissive approach. However, this does not mean that the reflective approach is only limited to the tile architecture and the transmissive approach is limited to the tray architecture. In fact, transmissive tiles are very common; on the other hand, reflective trays have yet to be reported.

For these two concepts, a tree diagram of promising spatial power combining structures is shown in Figure 5. Each approach presents two configurations that were potential candidates for use as a feed for the reflectarray. The following subsections describe these configurations.

10

Figure 4: Approaches to illuminate the reflectarray with the spatial power combining unit (a) Reflective approach; (b) Transmissive approach.

```
                    ┌─────────────────────────┐
                    │   FEED FOR REFLECTOR     │
                    │    Array configuration   │
                    └─────────────────────────┘
              ┌──────────────┴───────────────────┐
     ┌─────────────────┐              ┌─────────────────┐
     │    REFLECTIVE    │              │   TRANSMISSIVE   │
     │    Sub-array     │              │ Direct illumination │
     └─────────────────┘              └─────────────────┘
```

SINGLE LAYER TILE	MULTI LAYER TILE	TRAY (AND TILE)	TILE
- Increased unit cell size	- Reduced unit cell size	- Good heat dissipation	- Thermal issues
- Reduced aperture efficiency	- Increased aperture efficiency	- Patch or end-fire elements	- Patch elements
- Simpler to design and build	- Vias (or slots) required	- Perpendicular amplifiers	- Vias (or slots) required

Figure 5: Tree diagram of potential spatial power combining structures.

2.3.2. Reflective Single Layer Tile

The major advantage of using a single layer structure is the reduction of the complexity of fabrication since all the elements (mainly radiating elements and active devices) are on the same layer. However, this requires a larger unit cell, especially if different radiating elements are used for the two polarisations. The main disadvantages of a large unit cell are a lower radiation efficiency and beam shaping limitations. A passive single layer configuration was reported in [13].

2.3.3. Reflective Multi Layer Tile

In a multi-layer arrangement [14-16], the amplifiers would be placed on the back layer, behind the ground plane. This would allow for a smaller unit cell size, which would increase the efficiency of the system. However, the complexity of the structure would be increased since vias or slots in the ground plane would be necessary. This might be even more complicated if a thick ground plane were used. Using a single element with slot coupling would not be possible since the slot dimensions would be fairly large compared to the patch size at Ka band.

Nevertheless, this structure is worth further investigation and was chosen as one of the candidates to pursue in this project. Chapter 3 is dedicated to the study of the multi layer reflective tile.

2.3.4. Transmissive Tray (and Tile)

The transmissive tray proposed in this project was similar to the structures reported in [9] (transmissive tray and tile using broadside radiating elements) or [17] (transmissive tray only using end-fire elements). The transmissive tray is simply made of a stacked layer on which end-fire elements are present. It is mechanically less complex than the transmissive tray and tile, in which arrays of broadside elements fed using the tray architecture are added. This implies adding a transition between the patch and its amplifier(s), which requires careful

12

design and can possibly represent a challenge. On the other hand, the isolation is increased in the tray and tile approach, therefore the possibility of potential oscillation is reduced.

In the tray architecture, the amplifiers are placed perpendicularly with respect to the array of elements, which allows a reduction of the unit cell size. This structure would be much thicker compared to the other structures proposed, but this may be acceptable in certain applications. Furthermore, by keeping the amplification area open, fans can easily be mounted near the amplifiers in order to provide cooling. The metal structure where the amplifiers are mounted would also act as a heat sink. Due to these numerous advantages, the transmissive tray was chosen as one of the configurations to be developed for this project. It was decided to include patch elements in addition to the tray structure, which would increase the isolation due to the continuous ground plane perpendicular to the direction of propagation. The transmissive tray (as it will be called from now on) is further described in section 4.

2.3.5. Transmissive Tile

Another transmissive configuration makes use of a tile architecture, very similar to what is shown in Figure 3(a). This is a classical approach to achieve spatial power combining. Broadside radiating elements, usually patch antennas, are used as the input and output of the spatial power combining structure. Again, as for the case of the multi-layer reflective approach, the thick ground plane would represent a problem due to difficulty in coupling through the thick ground plane. As reported in [7-8], the heat dissipation represents a serious problem in this case and complex techniques must be used to cool down the structure.

2.3.6. Comparison of Technologies

The major advantages and disadvantages of the different technologies were reported in the previous subsections. In this section, Table II provides a summary for the two candidate configurations.

Table II: Comparison of the two spatial power combining configurations investigated in sections 3 and 4.

	Reflective multilayer tile structure	Transmissive tray structure
Architecture	Tile	Tray
Unit cell size	~ $1.0\lambda_0$	~ $0.7\lambda_0$
System thickness	Relatively thin (multilayer structure)	Thick (stacked structure)
Isolation	Good isolation due to orthogonal polarisation	Good isolation due to shielded system
Transition	Vias or slots through thick ground plane	Complex transitions (proximity feed, slot-to-waveguide-to-microstrip), vias
Heat dissipation	Fans and/or heat sink behind the reflective side, thick carrier structure	Fans on the side of the structure, multiple thick carrier structures
Impact on reflectarray	Reduced length compared to directly feeding the reflectarray	Increased length compared to dual-reflectarray configuration
Technology at Ka band	None reported	[9]

14

3. Reflective Multilayer Tile

In this chapter, the development of the reflective multilayer tile is reported. This mainly includes the design and analysis of the radiating element and array.

3.1. Single Element

The spatial power combining structure was made of broadside microstrip patch elements. Radiating patches were chosen because of their small size and ease of fabrication. Since this structure was composed of more than one layer, the active devices were not located on the same layer as the radiating elements; therefore transitions were required to couple the power between layers. Usually, it is simpler in terms of fabrication process to use slots in the ground plane to couple the power. However, in this case, a dual-fed patch was required, which made the use of slots more difficult since their size was quite large with respect to the patch size. Furthermore, since a thick ground plane was used in the active configuration (to help dissipate heat), the slot would therefore act as a waveguide, and would have to be carefully designed to avoid the cutoff region.

Instead of using slots in the ground plane, metallised vias were used. Because of their small diameters, it was possible to have two metallised vias relatively close to the middle of the patch and therefore obtain good isolation and good return loss using matching networks. Thus, the same technology was used for both a thin and a thick ground plane; however, the tuning of the matching network was different depending of the thickness of the ground plane.

Because of the size and close location of the vias, their fabrication resulted in a significant mechanical challenge. In this section, the design and results of a single element microstrip patch antenna on both thin and thick ground planes is presented.

3.1.1. Thin Ground Plane Design

The patch antenna was fabricated on a thin substrate material with a low dielectric constant in order to maintain the size of the patch as large as possible to allow for a dual-fed configuration. On the other hand, the feed layer was fabricated on a material with high dielectric constant to keep the feed lines thin and to allow the patch to be fed as close as possible towards the middle. The material description is provided in Table III. All metal layers were a few microns thin and were considered as infinitely thin in the simulations.

The patch antenna and the feed network were tuned using Ansoft Ensemble 8 [18]. Figure 6 shows a top view of a two-port dual-fed patch antenna. This antenna was fabricated in order to measure the return loss of each port, the isolation and the radiation patterns. The dimensions are provided in Table IV.

Table III: Material description for the multilayer patch antenna (thin and thick ground plane).

	Patch substrate	Circuit substrate
Name	Rogers RT/Duroid 5880	Rogers TMM10i
Thickness	10 mils (0.254 mm)[1]	15 mils (0.381 mm)
Dielectric constant	2.20	9.80
Loss tangent	0.0009	0.0020
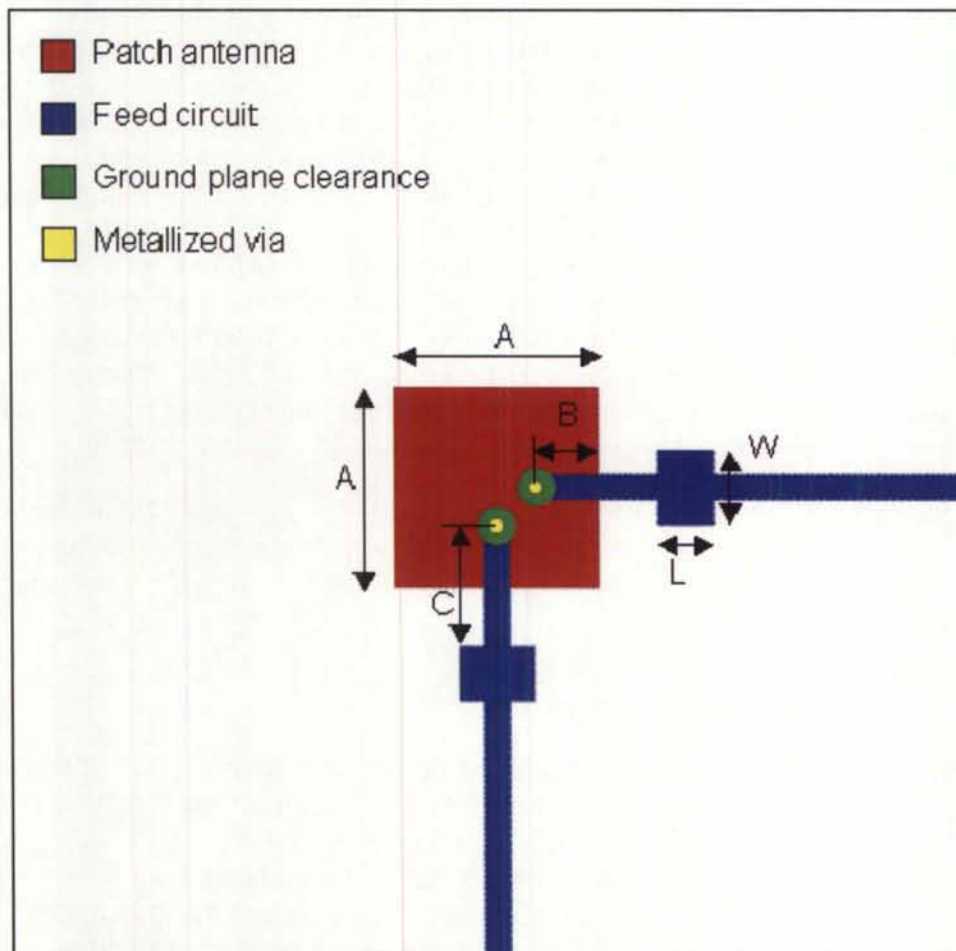
Figure 6: The dual probe-fed microstrip patch antenna on thin ground plane.

---

[1] In the simulations, the thickness of the patch substrate was assumed to be 11.5 mils (0.2921 mm) to take into account the thickness of the bonding sheet.

Table IV: Dimensions of the dual probe-fed patch antenna.

Description	Symbol	Thin Ground Plane (mm)	Thick Ground Plane (mm)
Patch size	A	3.2	3.05
Clearance hole diameter	—	0.6	0.6
Via hole diameter	—	0.2	0.2
Via-to-patch edge distance	B	0.925	1.525
Via-to-transformer distance	C	1.9	2.2
Quarter-wave transformer length	L	0.9	0.850
Quarter-wave transformer width	W	1.2	1.050

3.1.2. Thin Ground Plane Results

The measured and simulated S-parameters are presented in Figure 7. It is shown that the measurement results were very similar to the simulated ones. The measured radiation patterns at 29.7 GHz are presented in Figure 8. From these measurements, the gain of the element was about 5.25 dB.

3.1.3. Thick Ground Plane Design

In the active configuration, a thick ground plane was used for mechanical strength and thermal dissipation purposes. The thickness of the ground plane was 2.54 mm. The thin ground plane patch antenna reported in Section 3.1.1. was used as the starting point for the design of the thick ground plane antenna. The FDTD simulation package EMPIRE from IMST was used to simulate and tune the microstrip antenna and matching network. The same dielectric materials were used (see Table III). The layout is presented in Figure 9 and the dimensions are reported in Table IV. The patch size was slightly retuned to a dimension of 3.05 mm by 3.05 mm in order to resonate at the proper frequency. The quarter-wave transformer matching network was also slightly tuned. The via-to-patch edge and via-to-transformer distances were significantly different for the following reasons:

- The via running through the thick ground plane can be considered as a section of coaxial line having a given electrical length and characteristic impedance, therefore requiring a different location for the quarter-wave transformer;

17
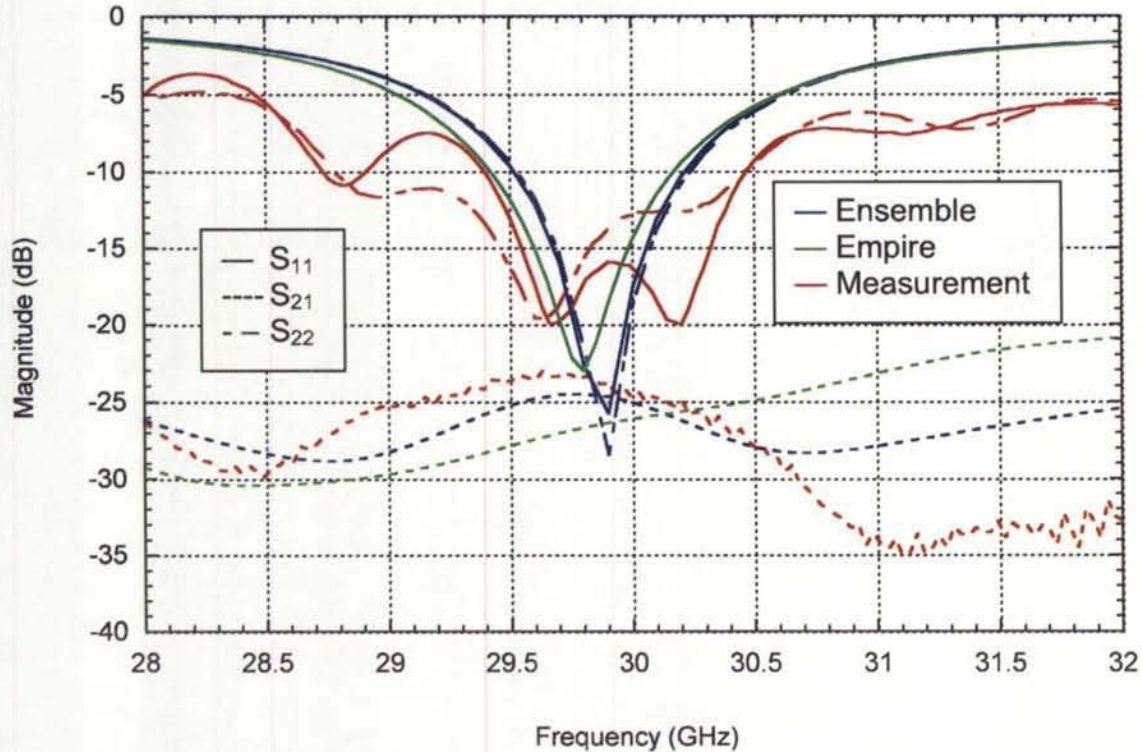
Figure 7: Measured and simulated S-parameters of the dual-fed patch antenna on thin ground plane ($S_{11} = S_{22}$ for Empire simulations).

- The horizontal polarisation was fed by a vertical transmission and vice versa, which was achieved to gain room in the final unit cell design (see Figure 9).

3.1.4. Thick Ground Plane Results

The measured S-parameters of the thick ground plane case are presented in Figure 10. The return loss was better than 14 dB and the isolation was better than -27 dB for the band of interest (29.5 GHz to 30 GHz). The measured radiation patterns at 29.75 GHz are presented in Figure 11 and show a gain of 5.7 dB.

3.2. Array Study

In order to feed the main reflectarray, an array made of the element designed in Section 3.1. was studied as a subreflectarray. There were many parameters related to this subreflectarray which had an impact on the maximum output power, gain, combining efficiency and shape of the beam:

18
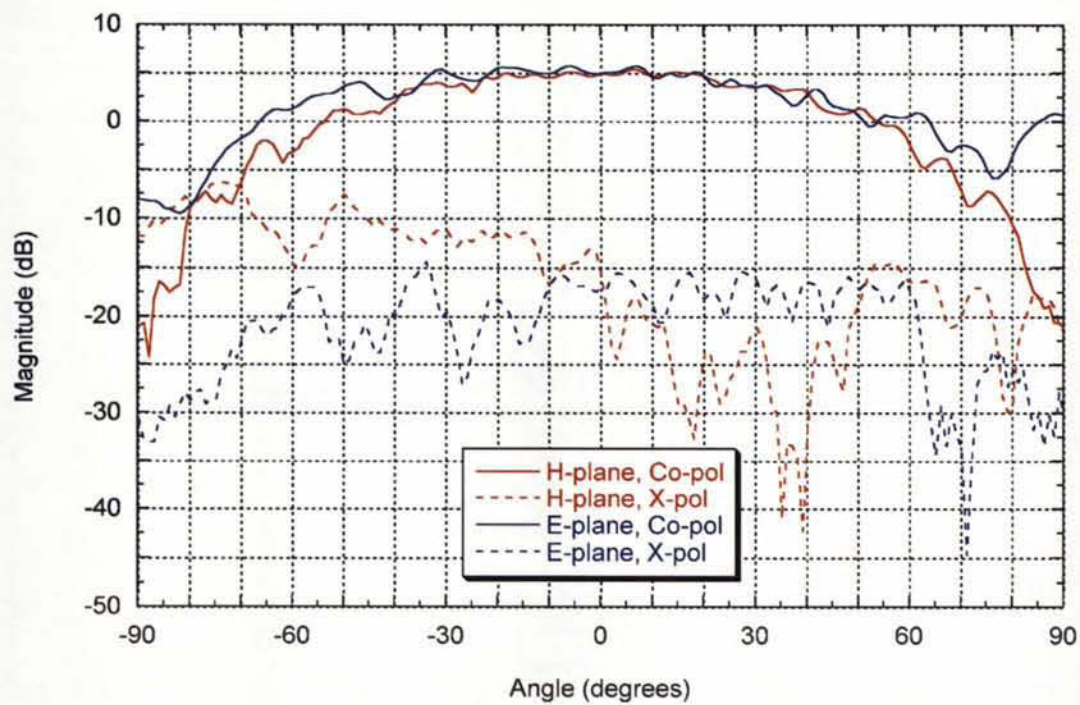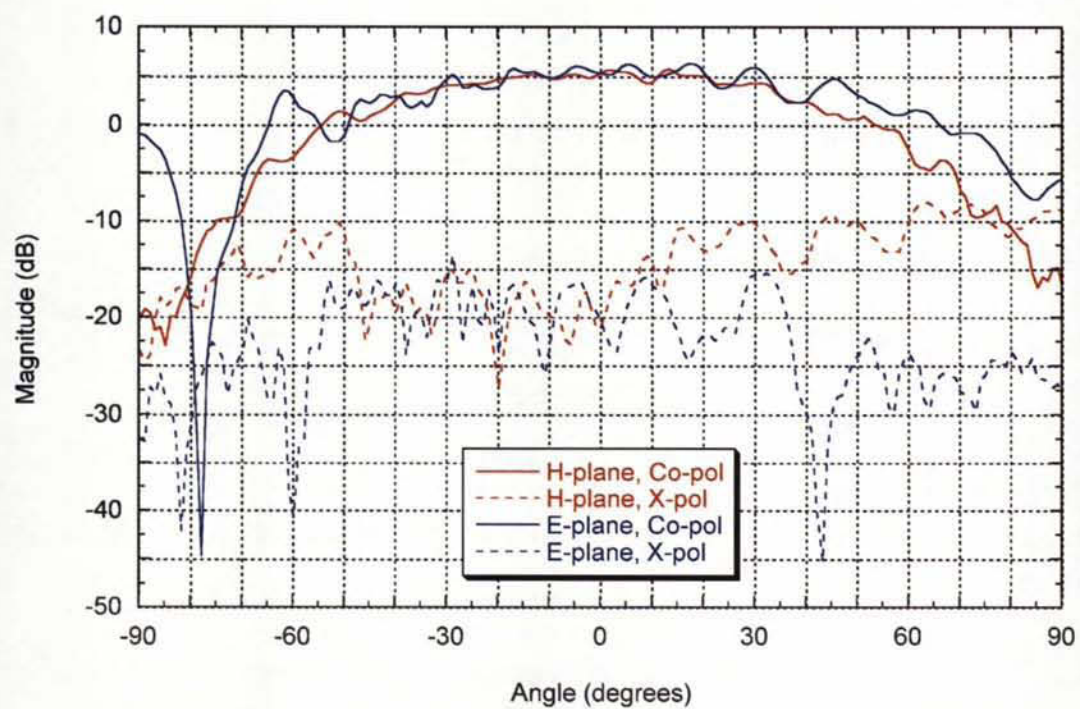
Figure 8: Far-field radiation patterns of the dual-fed patch antenna on thin ground plane (a) Port 1; (b) Port 2.
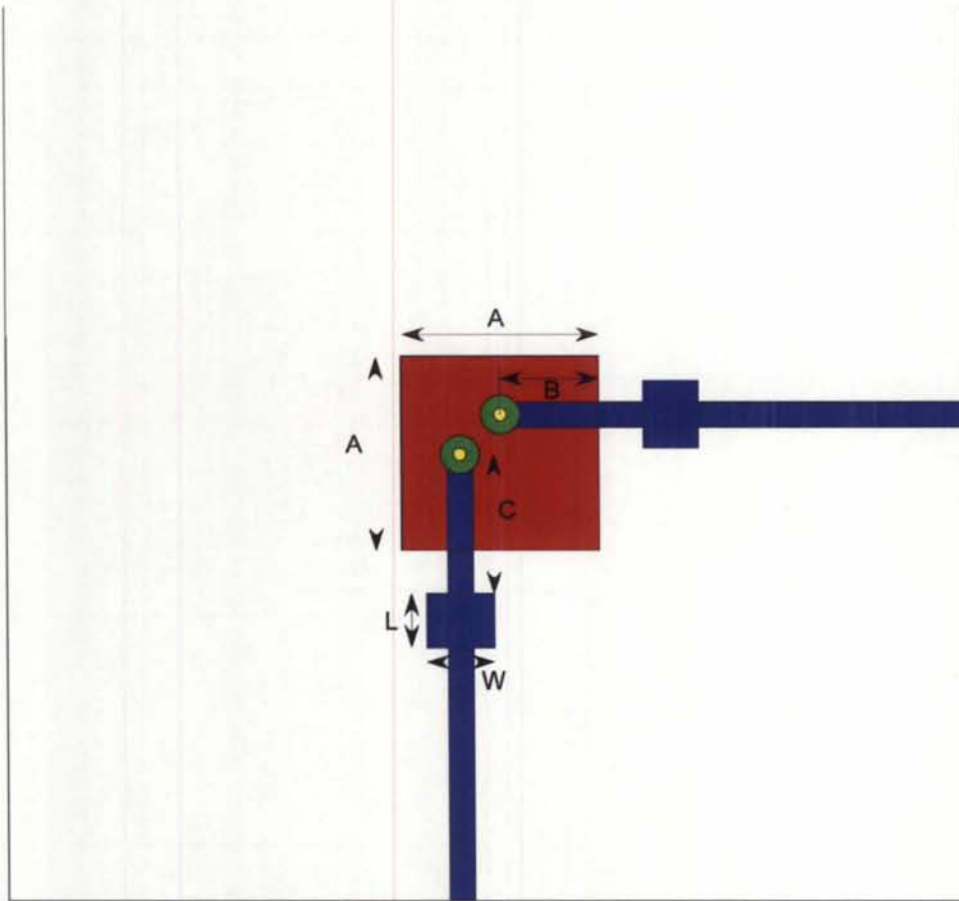
Figure 9: The dual probe-fed microstrip patch antenna on thick ground plane.

- The number of elements in the array;

- The shape of the array;

- The unit cell size (or the distance between the elements);

- The beam width and gain of the feeding element;

- The separation between the feeding element and the subreflectarray;

- The feed edge angle (or interception angle);

- The feed taper at the interception angle (and the power profile) and;

- The phase profile.

The following subsections explain in more detail the impact of all these parameters.
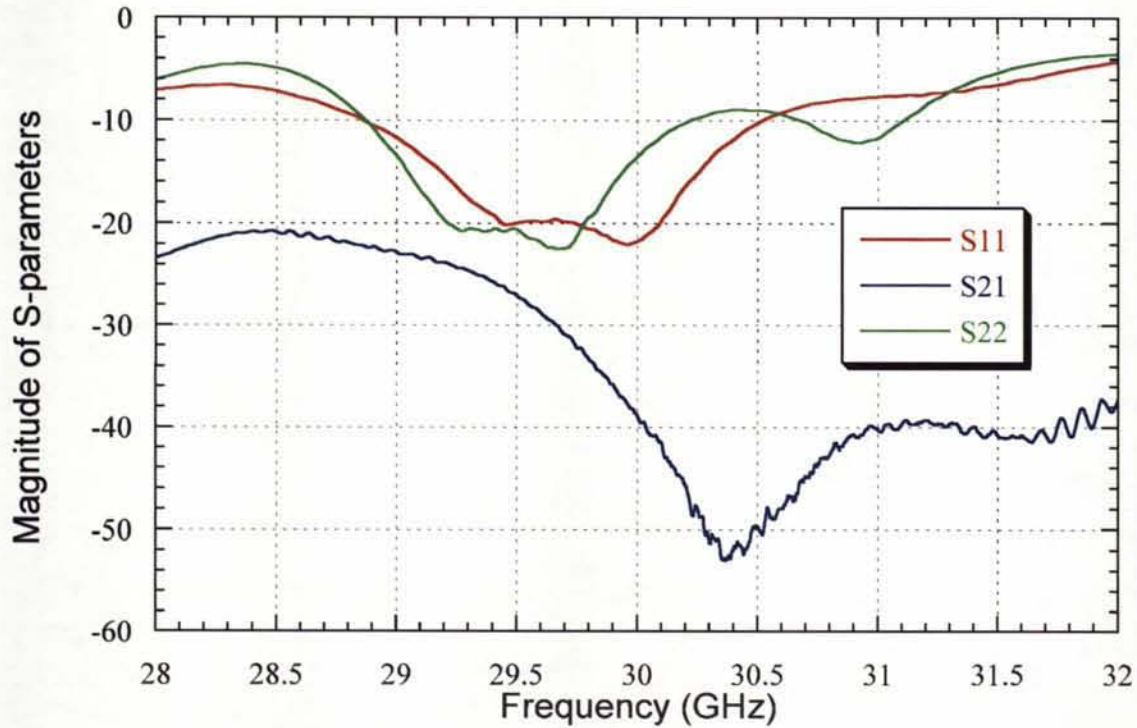
Figure 10: Measured S-parameters of the dual-fed patch antenna on thick ground plane.

3.2.1. Number of Elements

The number of elements is a crucial parameter of the array. In spatial power combining, each element of the array produces a certain output power. The power radiated from each element is then combined in free space. Therefore, the output power increases with the number of elements. However, if the size of the array is increased, this will result in higher blockage for the main reflectarray, therefore a smaller array would be preferred. Furthermore, a larger array usually has a larger feed taper value, therefore the combining efficiency is reduced since the elements on the edge of the array receive less power. A larger array also produces a narrower beam, which is not good as it increases the *F/D* ratio and requires a larger distance between the main reflectarray and the subreflecting spatial power combiner.

In summary, it was decided to design an array with sufficient elements to meet the output power requirements while keeping the array size as small as possible.
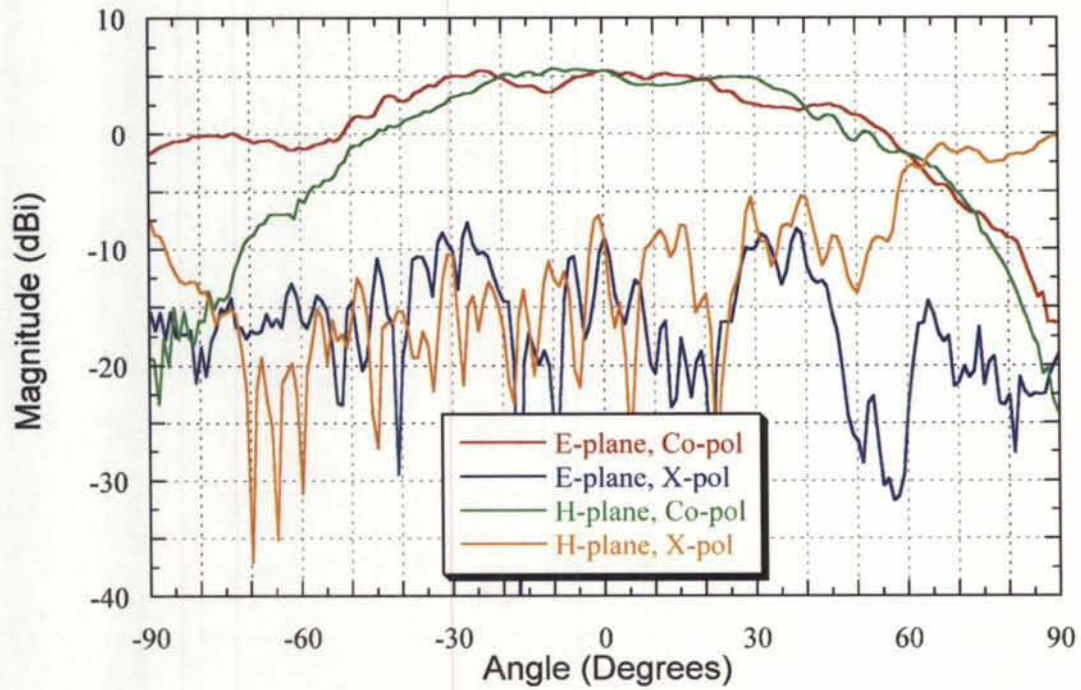
(a)
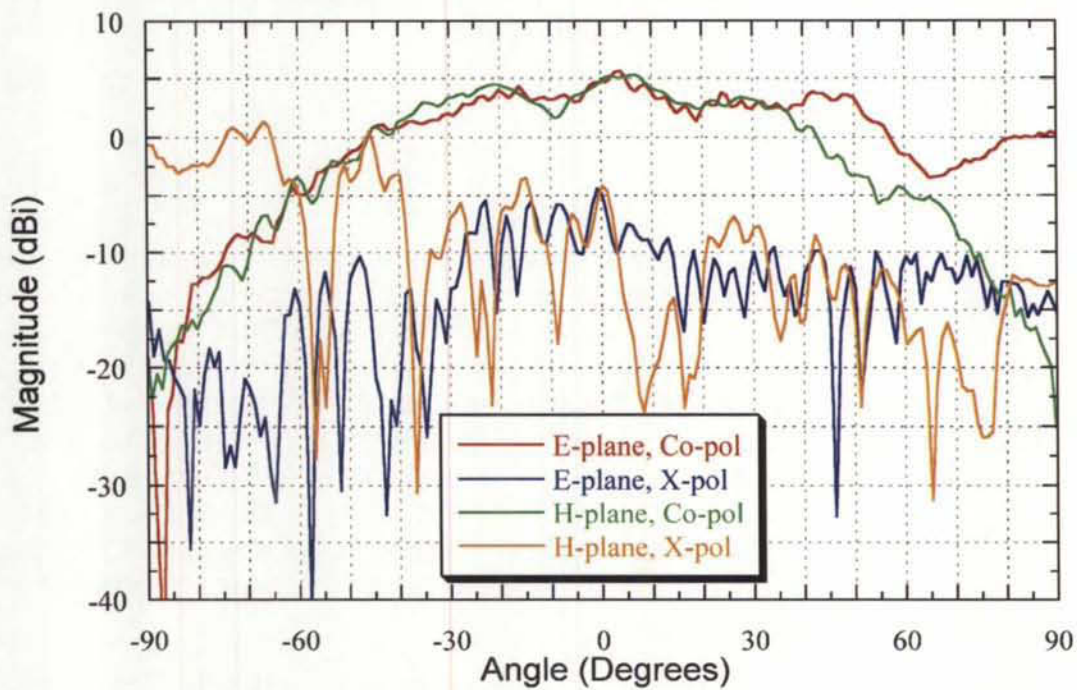
(b)

Figure 11: Far-field radiation patterns of the dual-fed patch antenna on thick ground plane (a) Port 1; (b) Port 2.

22

3.2.2. Unit Cell Size

The unit cell size is the area occupied by a single element of the spatial power combining array. It can also be taken as the distance between two adjacent elements of the array, from centre to centre. In terms of array performance and beam shaping capabilities, this distance should be kept as small as possible, but not too small since this would create mutual coupling between the elements. A large unit cell size usually creates many nulls in the radiating patterns and problems while attempting to shape the beam, either with power or amplitude variation. Furthermore, smaller unit cell size allows for a higher power concentration, therefore a higher combining efficiency.

In designing spatial power combining systems, it is usually difficult to achieve a small unit cell size due to the large area occupied by the radiating elements and the active devices.

3.2.3. Feeding Element

The feeding element (or feed horn) usually dictates the power profile. This will be discussed later on in subsections 3.2.4. and 3.2.5. However, the subtended angle of the feed beam, the feed beam taper and the power profile, which are interdependent parameters, can be adjusted by changing the location of the feed horn.

One of the problems that can occur for a low-gain horn is that one would require placing the feed horn very close to the spatial power combiner, thus resulting in larger blockage for the subreflecting spatial power combiner and also a possible problem achieving maximum output power if the required input power cannot be obtained due to the lower gain.

3.2.4. Feed Taper at the Interception Angle

The feed taper dictates the power level (relative to the maximum power level) at a certain angle, usually the interception angle. The interception angle is half of the angle measured from the feed horn which is subtended by the edge of the subreflecting surface.

If the feed taper is large, the spillover at the subreflector is low, which leads to a high spillover efficiency. Considering a reflector with fixed size, these configurations have smaller separations between the feed horn and the subreflector, which translate to a lower path loss due to a shorter distance between the feeding element and the sureflectarray. Thus, the maximum output power for the amplifier requires less amplifier gain to be obtained (this is only true for the elements close to the centre). Consequently, the overall amplifier gain has to be reduced to avoid saturation. Furthermore, the large taper results in a significant difference in terms of power between the centre elements and the

edge elements, which allows for a wider beam and less ripples to illuminate the main reflector.

However, with a large feed taper, the taper efficiency would be reduced and most of the amplifiers would not receive enough input power to produce maximum output power (the shortcoming can be circumvented by using amplifiers with more relaxed power handling and gain specifications as the edge region is approached, however this would imply using driver amplifiers and different DC biasing networks, both of which are undesired in order to save on real-estate, cost and complexity). Consequently, the overall output power is reduced and so is the combining efficiency. Table V presents the effect on the various parameters for small and large feed taper.

3.2.5. Phase Profile

It is possible to shape the beam radiated by the subreflectarray. This is done by changing the power or the phase at the elements of the subreflecting spatial power combining array. However, the power profile is essentially dictated by the beam shape of the feed horn as it is very difficult to change the power produced by each element. This would require a different gain for each amplifier, thus different biasing and possibly different devices, which is not a very practical solution.

However, the phase profile can be changed easily by changing the length of the line for the different elements of the spatial power combining array. This allows increasing the width of the beam. However, there are some limitations since a large phase difference between the elements results in high ripples in the radiation pattern and possibly nulls.

3.3. Array Design

With the knowledge provided in Section 3.2., the design of the spatial power combining array is presented in this section.

3.3.1. Feed Horn

In order to feed the subreflectarray, a feed horn was chosen. The choice had to be made between existing feed horns of 14 dB and 20 dB. Since it was preferable to illuminate the subreflectarray with as high a power density as possible, it was decided to choose the 20 dB gain feed horn.

A few calculations were also performed assuming that a planar quad-patch antenna was used as the feed, which could be located on the same layer as the main reflectarray. Having the feeding antenna and the main reflectarray on the same layer would faciliate fabrication, allowing both the feed antenna and the main reflectarray to be made during the same process and also result in a

Table V: Effect of the various parameters with feed taper.

Parameters	Small feed taper	Large feed taper
Spillover efficiency	Low	High
Taper efficiency	High	Low
Beam width	Small (not significant)	Large (not significant)
L/D ratio and F/D ratio	Large (not significant)	Small (not significant)
Ripples in radiation pattern	High	Low
Horn-subreflectarray separation	Large	Small
Amplifier gain required	High	Low
Achievable output power	High	Low
Combining efficiency	High	Low

two-component system (combined main reflectarray and feed, plus subreflectarray) as opposed to a three-component system (main reflectarray, subreflectarray and feed horn). This would result in a less complex mechanical structure. Unfortunately, because of the large separation distance between the subreflectarray and the main reflectarray, the power received by the subreflecting spatial power combiner would have been quite low when the feeding antenna was printed on the main reflectarray, thus the overall output power would have been lower than desired. It was then decided to keep a three physical component configuration.

3.3.2. Feed Taper and Interception Angle

Different feed tapers were tested in order to find the optimum value for illuminating the power combining array. Even though it was shown that lower feed taper values result in greater output power, the gain required by the amplifiers would have been quite high. Using a 3 dB taper illumination across the spatial power combining array, it is theoretically possible, with a TriQuint TGA4509-EPU MMIC, to reach the maximum device output power without the need for a driver amplifier. For smaller amounts of taper using the same feed horn, the separation between the horn and the subreflectarray would have to be increased, resulting in higher free-space path loss and necessitating driver amplifiers

3.3.3. Active Device Properties

To achieve an output power between 15 W and 20 W, high-power MMIC devices were required. Typically, 1 W devices or more should be used. Assuming the combining efficiency was about 50%, 30 to 40 elements would be required to reach the desired power. For higher output power, say 2 W devices, about half the number of amplifiers would be needed.

The advantage of using 1 W amplifiers compared to higher-power amplifiers is that the 1 W devices are relatively small, therefore the overall unit cell size was reduced. Moreover, these devices produce higher gain and they were much less expensive than the ones producing higher output power.

The best candidate for the current project was chosen to be the TriQuint TGA4509-EPU 1 W power amplifier. The specification sheet of this device is provided in Appendix A. The device was measured in house and the measurement results are presented in Figure 12.

3.3.4. Subreflectarray Size and Shape

As mentioned in the previous section, the array should be made of about 30 to 40 elements. One approach was to use a 6 × 6 element array; however there were other possibilities for non-square shapes. A 6 × 6 element array would be a more suitable choice for a tray architecture.

For the reflective tile, the 37-element array configuration, shown in Figure 13, was proposed. This configuration allowed for a more uniform illumination of the outer elements, since their distance to the feed was nearly the same. For the square lattice case, the corner elements would be farther away from the centre and would receive very little incident power, making their contribution negligible.

3.3.5. Unit Cell Size

The unit cell size had to be kept as small as possible, but not too small though since the radiating patch elements might interfere with each other. However such interference might not be possible in this case because of the area to be occupied by the patch element, the active devices and other components. In the actual case, the goal was to obtain a unit cell size of one wavelength at 30 GHz, i.e. 10 mm. Section 3.4 provides more detail on the active unit cell.

26
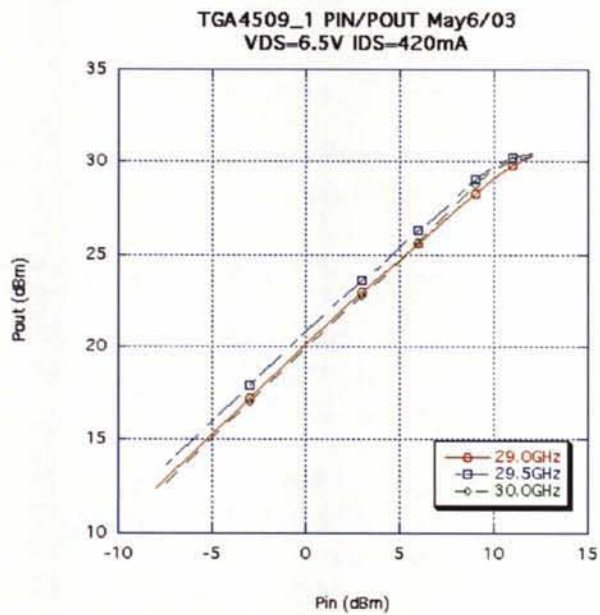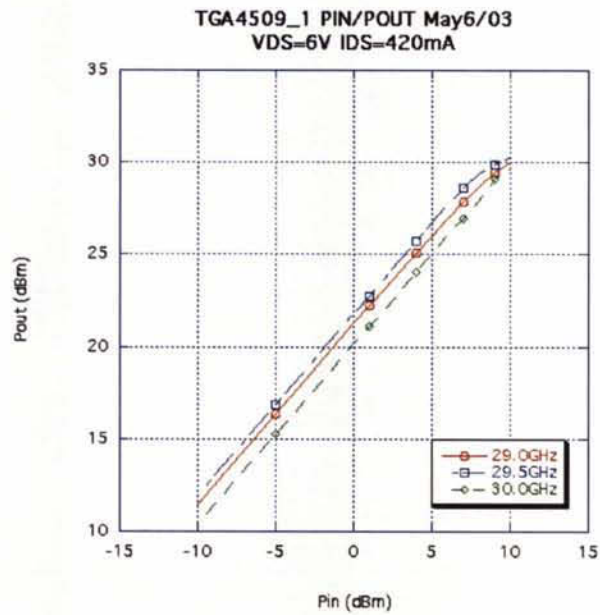
Figure 12: Output power vs input power for the TriQuint TGA4509-EPU power amplifier
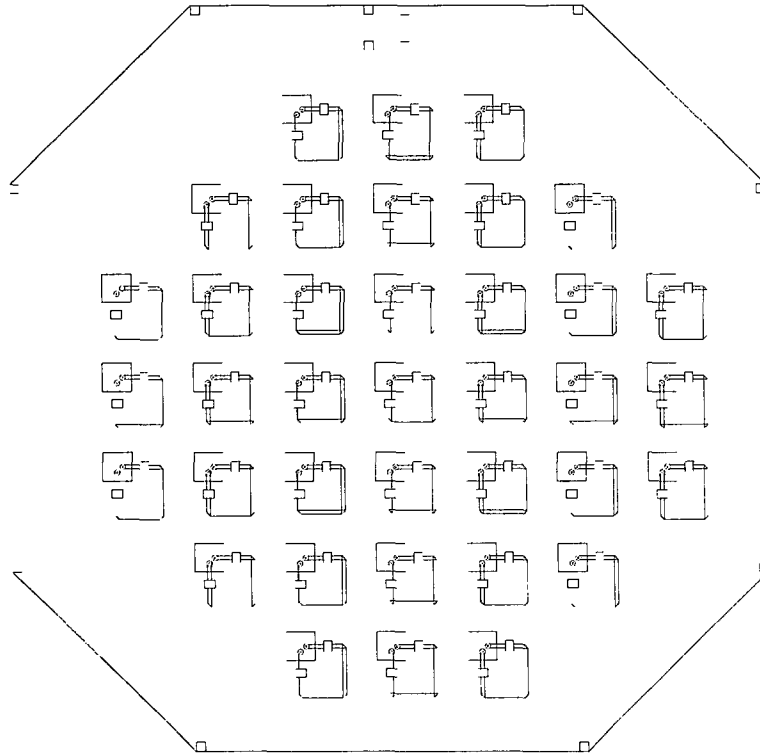
Figure 13: 37 element array configuration (passive array).

3.3.6. Iterative Process for Phase Compensation

When all the previous parameters were finalized, the shape of the required beam reflected by the spatial power combining array was determined. Then, the phase of the each element in the array was adjusted in order to obtain this desired beam shape. This iterative process was carried out using a Mathcad [19] script, RASCAL [20] and ARPS [21]. First, the diameter of the main reflectarray was fixed and an approximate value for the distance between the subreflectarray and the main reflectarray (also called antenna length) was assumed. The following procedure was then used:

- RASCAL was used to model the reflectarray and the subreflectarray with a conventional parabolic main reflector and hyperbolic subreflector. The same dimensions were assumed. Then, all the known parameters were entered into the software (main reflector diameter, subreflector diameter, assumed antenna length, feed edge angle and feed taper).

- From RASCAL, some geometrical parameters were obtained, mainly the eccentricity and the interfocal distance.

- These parameters were then plugged into the Mathcad script and were used to calculate other parameters, like the distance between the feed horn and the subreflectarray (also called separation).

28

- A phase compensation process was then initiated in the Mathcad script to take into account the phase introduced by an ideal hyperbolic subreflector and then translate this phase to each element of the subreflectarray. This was the starting point for the phase compensation.

- ARPS was used to estimate the pattern shape of the reflected beam from the subreflectarray when the phase was modified in order to widen the beam width, and therefore reduce the antenna length. The new phase profile was found from a second-order equation of the form

$$\phi = ad^2 + bd ,$$ (5)

where ϕ is the phase, a and b are the equation parameters and d is the distance between the centre of the array and the radiating element being considered. Such a phase profile is similar to the one introduced by the hyperbola, however the parameters are then varied. Good performances were obtained by varying a only while fixing b to zero.

- From the beam shape obtained in ARPS, a value of feed taper at the main reflectarray was chosen. In this case, 10 dB was chosen since it was close to the optimal efficiency of the reflectarray (based on the spillover and taper efficiencies). Therefore, the beam width of the subreflecting array for this feed taper, as estimated by ARPS, was used to calculate the antenna length. This new value of antenna length was then used in RASCAL and the iterative process starts again.
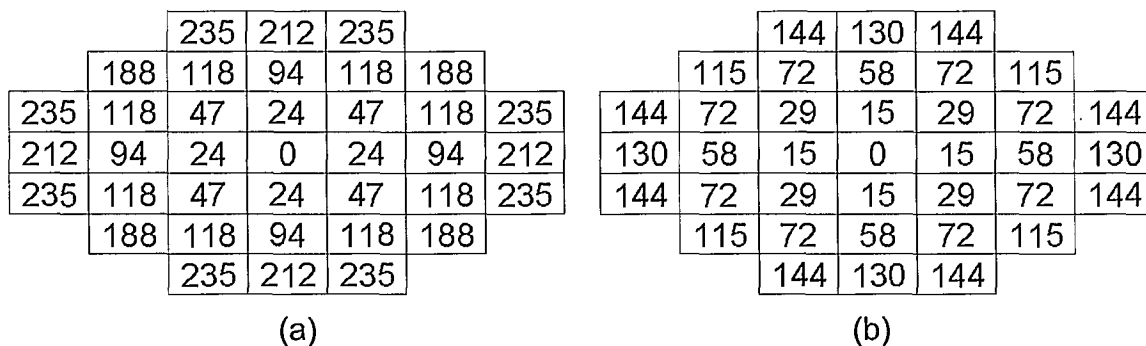
This method usually converged within 3 or 4 iterations. If the initial guess value was close to the value obtained in RASCAL, then only 2 iterations were necessary.

The phase profile obtained using this technique is shown in Figure 14(a). Figure 14(b) shows the phase profile to be introduced at each element, accounting for the effect of the feed horn phase. The power profile, which is essentially dictated by the feed horn illumination, is shown in Figure 15. The resulting radiation patterns of the array simulated with ARPS is shown in Figure 16.
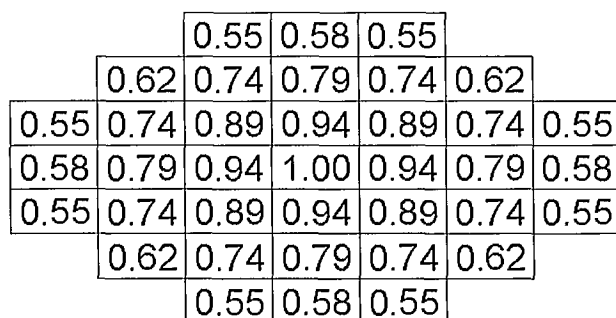
3.3.7. Figures of Merit Calculation

After the power profile was determined, parameters and figures of merit which are characterizing the spatial power combiner were calculated. Knowing that the gain of each receiving element, G_{A_Rx}, was 5.25 dB, the effective area, A_{A_Rx}, was calculated using:
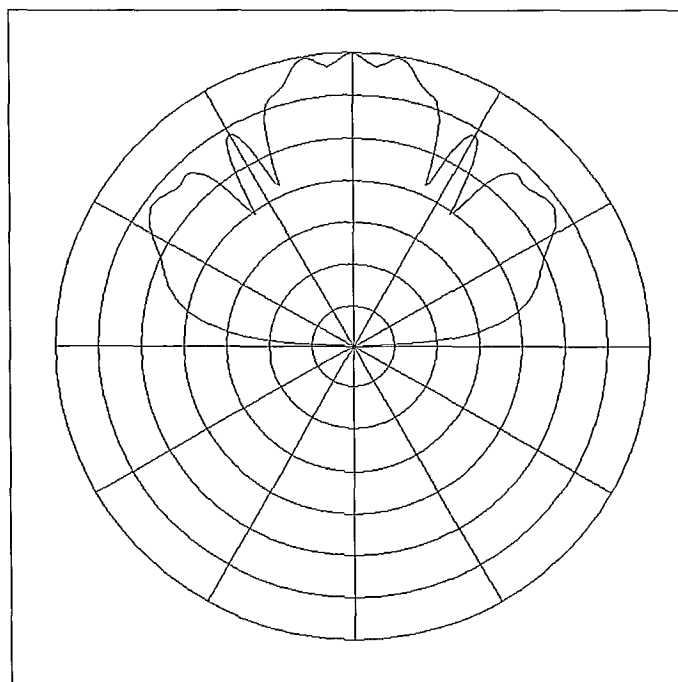
$$G_{A\_Rx} = \frac{4\pi A_{A\_Rx}}{\lambda^2} .$$ (6)

29

		235	212	235		
	188	118	94	118	188	
235	118	47	24	47	118	235
212	94	24	0	24	94	212
235	118	47	24	47	118	235
	188	118	94	118	188	
		235	212	235		

(a)

		144	130	144		
	115	72	58	72	115	
144	72	29	15	29	72	144
130	58	15	0	15	58	130
144	72	29	15	29	72	144
	115	72	58	72	115	
		144	130	144		

(b)

Figure 14: Phase profile (in degrees) for each element of the array with respect to their position (a) without considering the effect of the feed horn; (b) by taking into account the phase introduced by the feed horn.

		0.55	0.58	0.55		
	0.62	0.74	0.79	0.74	0.62	
0.55	0.74	0.89	0.94	0.89	0.74	0.55
0.58	0.79	0.94	1.00	0.94	0.79	0.58
0.55	0.74	0.89	0.94	0.89	0.74	0.55
	0.62	0.74	0.79	0.74	0.62	
		0.55	0.58	0.55		

Figure 15: Relative power profile for each element of the array.

Figure 16: Radiation pattern for the array.

In (6), λ is the free-space wavelength.

The input power for each amplifier, $P_{in\_amp\_x,y}$, was calculated using

$$P_{in\_amp\_x,y} = \frac{P_{in}G_{Tx\_x,y}A_{A\_Rx}}{4\pi Dist_{x,y}^{2}}, \tag{7}$$

where $Dist$ is the distance array and

$$\frac{G_{Tx\_x,y}}{Dist_{x,y}^{2}} \propto P_{profile}, \tag{8}$$

where $P_{profile}$ is the power profile, as shown in Figure 15. The total output power, P_{out}, was calculated as follow:

$$P_{out} = G_{amp}\left(10^{\frac{IL}{20}}\right)\sum_{x}\sum_{y}P_{in\_amp\_x,y}, \tag{9}$$

where G_{amp}, the gain of the amplifier, was 22 dB and IL, the insertion loss at the amplifier output, was assumed to be 2 dB.

The calculated output power was 18.31 W and the combining efficiency was 49.47 % assuming 1 W at the input of the feed horn. The corresponding gain of the spatial power combiner was then 12.63 dB. However, in this situation, the maximum output power for a single device was less than 1 W, the maximum output power of a single amplifier. To achieve 1 W, an input power at the feed horn of 1.15 W had to be applied, in which case the output power of the spatial power combiner was 21.05 W and the combining efficiency was 56.89 %. Table VI presents these results.

3.3.8. Passive Array Results [1]

The passive subreflector of Figure 13 was fabricated and measured in order to verify the validity of the magnitude and phase profiles. Photographs of this subreflectarray are shown in Figure 17. The desired goal was to achieve an edge taper of 10 dB on the main reflector. The measurements were performed using a planar near-field scanner on just the feed horn and the subreflector with the feed horn facing the subreflector, as shown in Figure 4(a), (the main reflector was not present). The near field was probed at a location L = 60 cm from the subreflector, i.e. at the intended location for the main reflector. Figures 18 and 19 show the results at 30 GHz. In Figure 19, the black contour represents the 10 dB edge taper and the white square represents the main reflector, which was assumed to be a square of 50 cm by 50 cm. In Figure 19, it is seen that the edge taper is close to 10 dB. The passive microstrip-array subreflector thus provides a satisfactory illumination for the main reflector.

**Table VI: Theoretical results for the spatial power combiner.**

| Parameter	Symbol	Case 1	Case 2
Input power	P_{in}	1 W	1.15 W
Number of elements	n	37	37
Separation	R	19.69 cm	19.69 cm
Subreflector feed taper	T_f	3 dB	3 dB
Edge angle	θ_e	10°	10°
Subreflector efficiency	η_a	75.44 %	75.44 %
Patch antenna gain	G_{A_Rx}	5.25 dB	5.25 dB
Amplifier gain	G_{amp}	22 dB	22 dB
Amplifier output power	P_{out}	1 W	1 W
Insertion loss	IL	2 dB	2 dB
Total output power	P_{out}	18.31 W	21.05 W
Combining efficiency	η_{comb}	49.47 %	56.89 %
System gain	G_{sys}	12.63 dB	12.63 dB

3.4. Active Unit Cell [1]

For the patch antennas described previously, the unit cell consisted of a dual-polarised patch that amplified the incoming signal from the feed horn. The amplified outgoing signal was retransmitted with a polarisation orthogonal to the incoming signal polarisation. This arrangement minimized the interference between the incoming and outgoing signals.

3.4.1. Unit Cell Description

A top view representation of the unit cell is shown in Figure 20. A three-dimensional view is shown in Figure 21. Figure 22 shows a photograph of an empty unit cell carrier. Each unit cell was built separately on a thick carrier module of 10 mm by 10 mm area. Afterwards, the cells were assembled at the end to form the active subreflector. The actual size was the minimum achievable
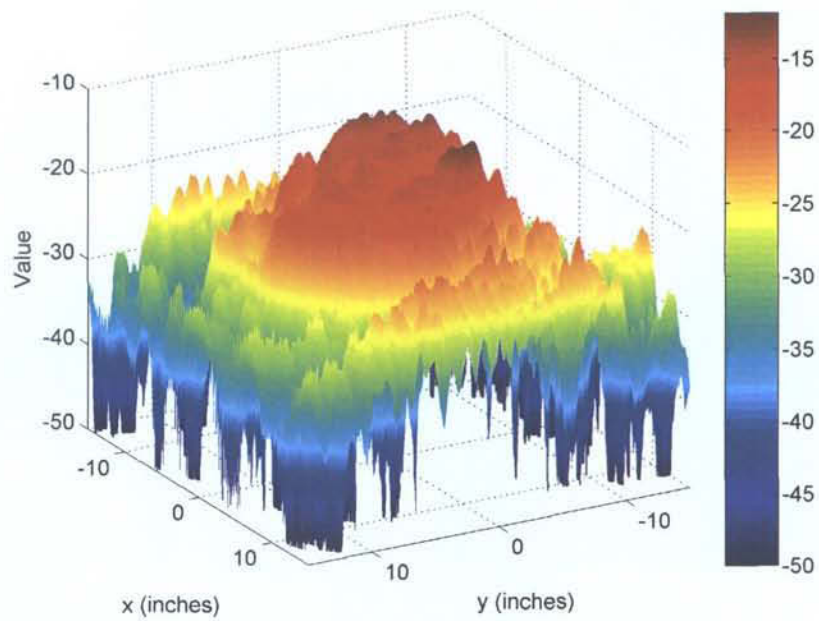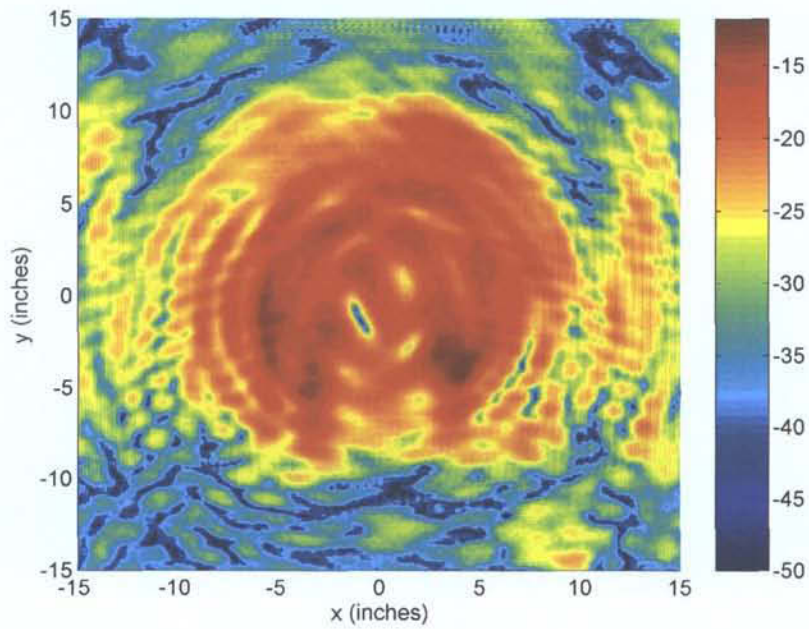
32
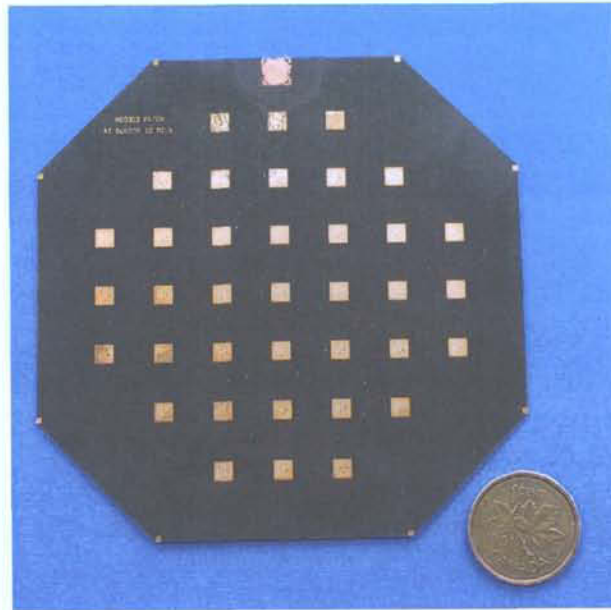
(a)
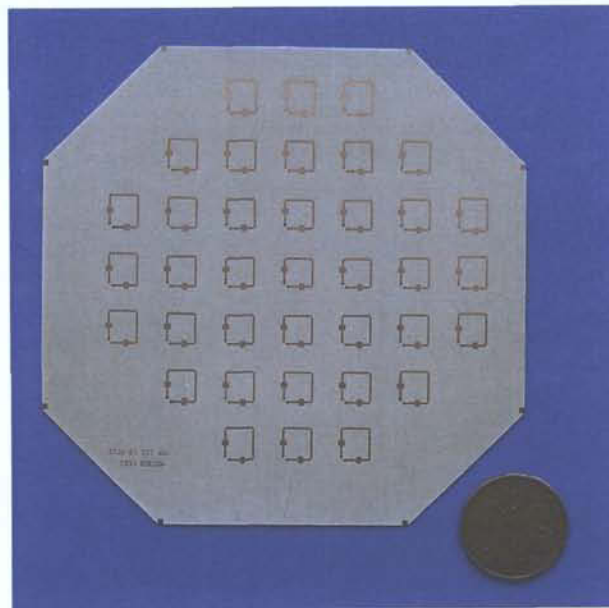
(b)

Figure 17: Photographs of the subreflectarray; (a) patch side view; (b) circuit view.

(a)

(b)

Figure 18: Power distribution at the main reflector; (a) Three-dimensional, (b) Contour plot.
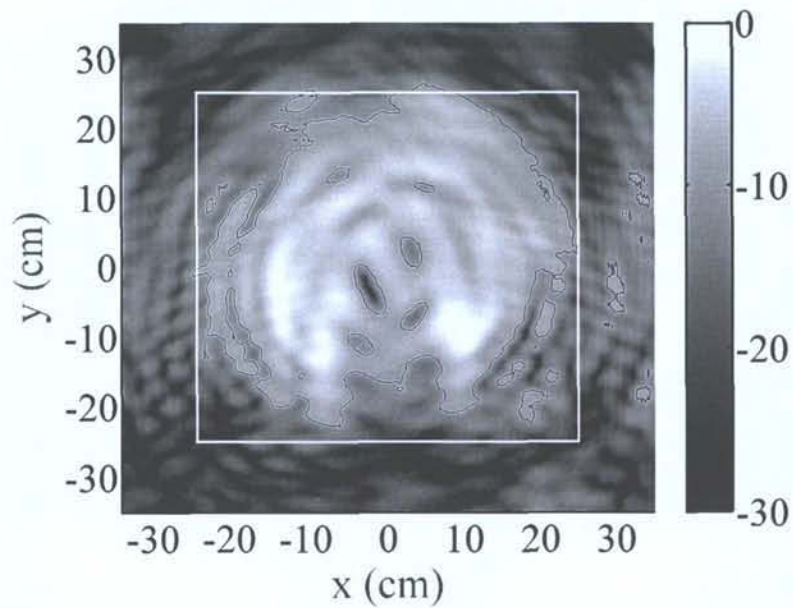
34

Figure 19: Power distribution at the main reflector (contour plot) with emphasis on 10-dB edge taper (black contour) and main reflector dimensions (white square).
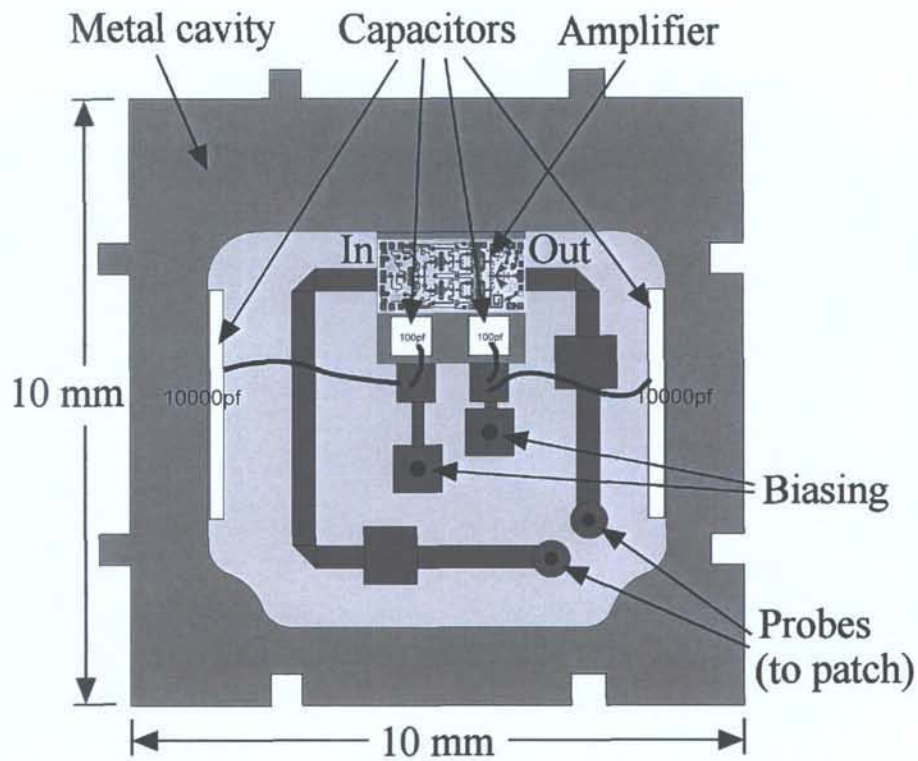
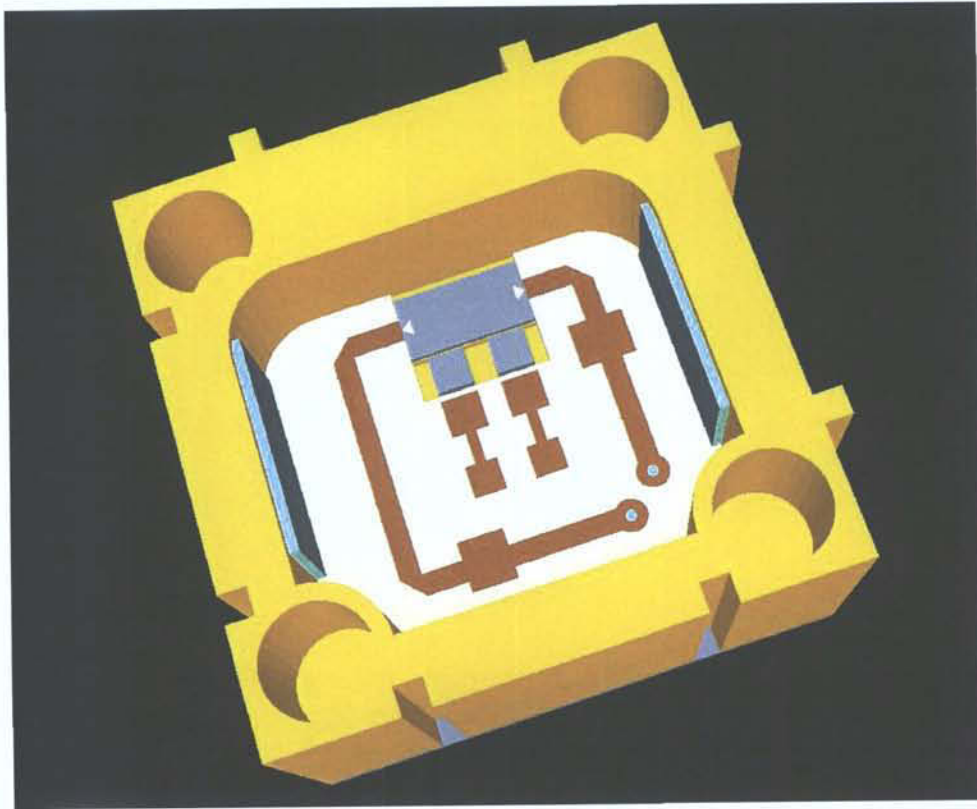

Figure 20: Top view of the active unit cell (RF circuit).

35

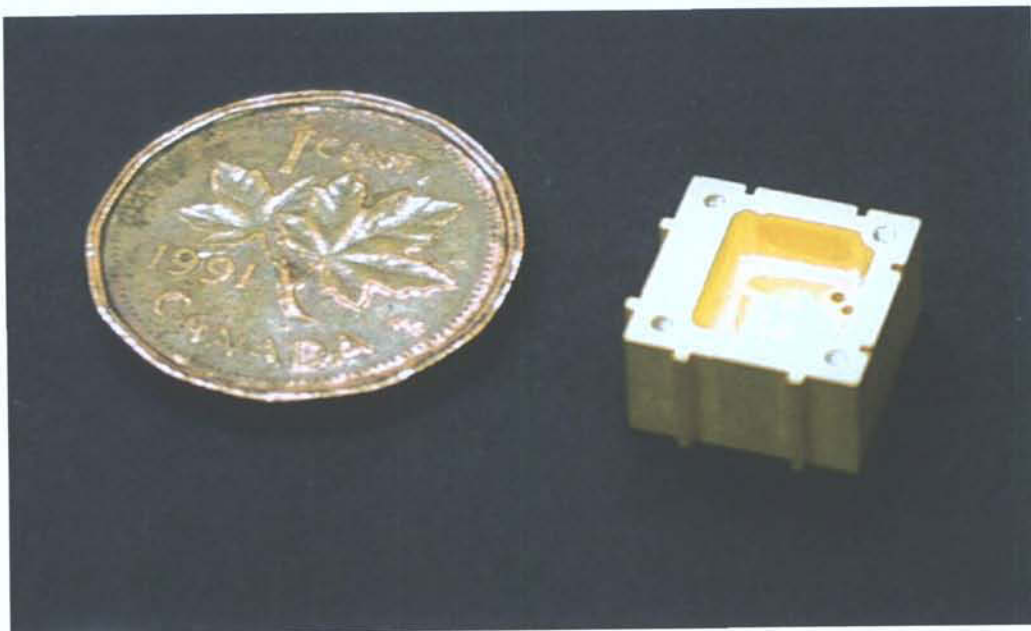**Figure 21: Three-dimensional representation of the active unit cell (RF circuit).**

Figure 22: Photograph of a carrier unit cell.

size considering all the components to be inserted in this unit cell: patch antenna, chip amplifier, microstrip transmission lines, biasing chip capacitors and DC biasing network. A modular approach was chosen to facilitate replacement or repair of the elements if a failure were to occur.

As mentioned in subsection 3.1.3., the patch antenna area was 3.05 mm by 3.05 mm and it was etched on a 0.254 mm thick substrate with a dielectric constant of 2.2. The ground plane thickness was 2.54 mm. A thick ground plane was used for mechanical strength and thermal dissipation purposes. Coaxial probes of inner diameter 0.2 mm and outer diameter 0.6 mm were used to feed the antenna. Their location was chosen to maximize the isolation between ports. The amplifier and transmission lines were located on the other side of the ground plane, inside a cavity. The width of the transmission lines was 0.4 mm and the substrate used had a thickness of 0.381 mm and a dielectric constant of 9.8.

Inside the cavity, two small 100 pF capacitors were located at the bottom and two larger 0.01 µF capacitors were mounted vertically, along the cavity walls. This was done to reduce the size of the unit cell. The cavity was then sealed with a lid, which was used both as a heat sink and a support for the biasing network.

### 3.4.2. Single Unit Cell Measurement

A single unit cell was originally built and DC tests were conducted. In the original design, oscillation occurred due to a lack of isolation between the input and output ports of the amplifier. The minimum isolation was 20 dB; since the gain of the amplifier was 22 dB, the isolation should have been increased by at least 2 dB.

With this design, the isolation could only be improved by moving the patch probes closer to the centre, which was not possible since the probes were already at the optimal physical location. Therefore, it was decided to add absorber on the input microstrip transmission line in the unit cell to reduce the coupling and avoid oscillation. Two non-conductive silicone absorbing pieces were then added on the input line.

Since the absorbing pieces also resulted in insertion loss and phase shift, they had to be of the exact same size and located at the same location for all unit cells in order to produce the same effect. Therefore, the magnitude and phase profile was kept constant for the array. The additional insertion loss resulted from the absorbing pieces was about 6 dB.

3.5. Four-Element Array Measurement [1]

A 2 × 2 element prototype array was built and tested. Figures 23 and 24 show the four-element array under measurement. The unit cells were chosen to have the same length of microstrip line for both input and output transmission
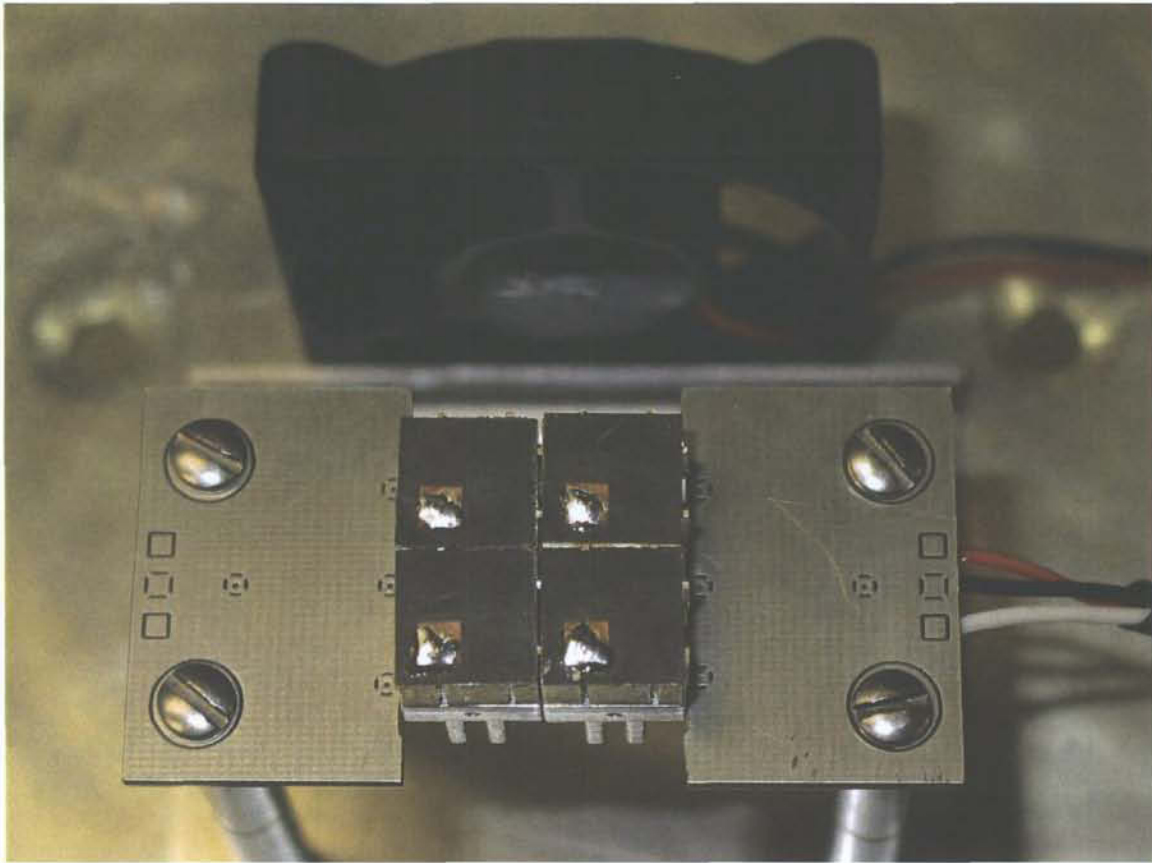
Figure 23: Photograph of the four-element array (top view).

lines, which resulted in the same phase for all unit cells. Absorbing pieces were inserted to improve the isolation, as described in the previous section. The array was measured in the far-field in order to apply the Friis equation. Since the active array was reflective, two pyramidal horns, identical to the one to be used to illuminate the reflective array in the final stage, were used. The horns were set up for orthogonal polarisation with the horizontally polarised horn transmitting and the vertically polarised horn receiving. The isolation between the horns was better than 54 dB for the band of operation, which was high enough to ensure it would not impact the measurement results. The distance between the pyramidal horns and the active array was 30 cm.

The 4-element array was measured in the operating band at three different frequency points. Table VII gives a summary of the measurements. The measured output power was obtained using a power meter; the ideal output power was calculated using the Friis equation according to the input power of the measurement setup.
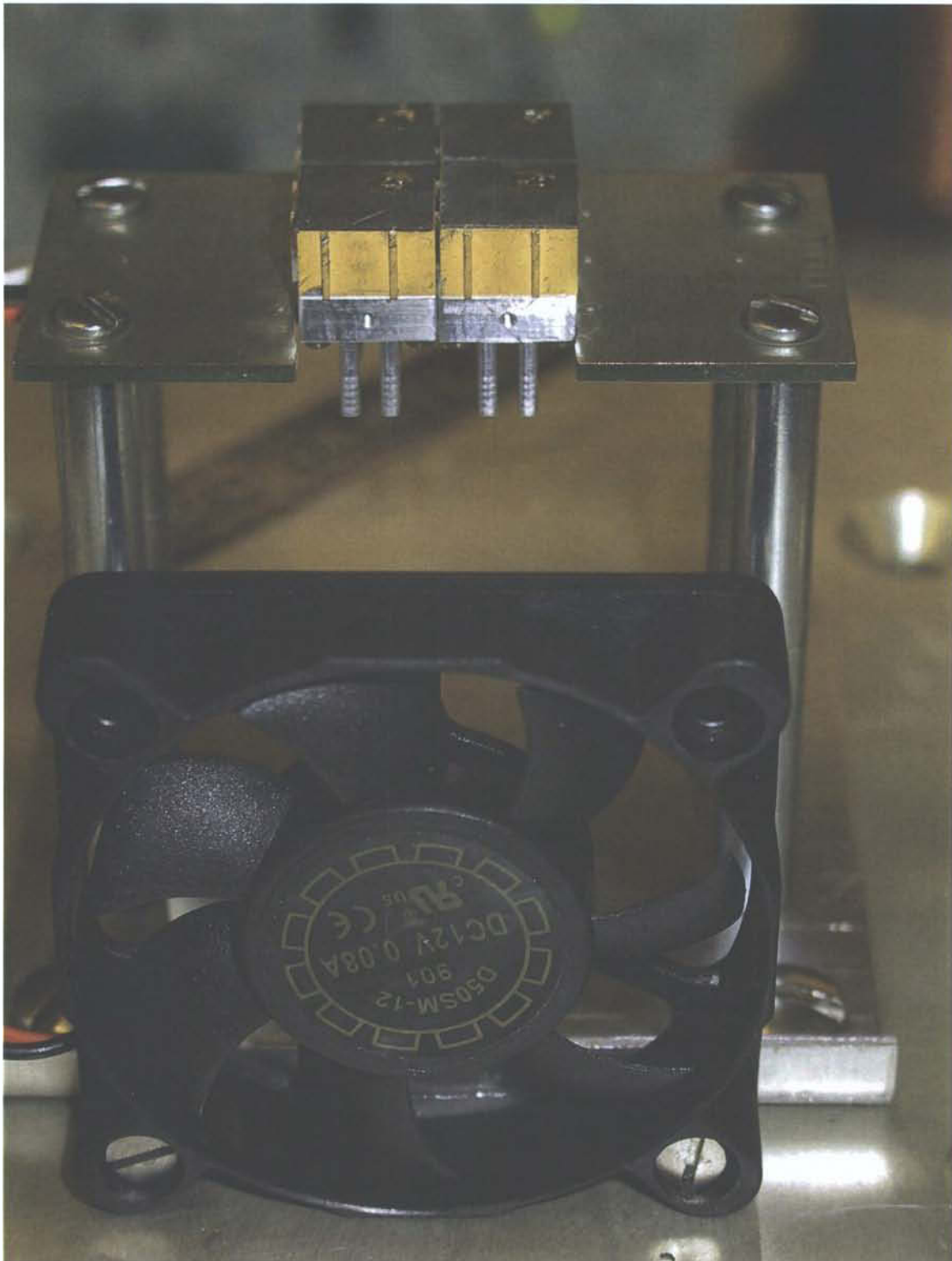
Figure 24: Photograph of the four-element array (side view).

Table VII: Output power results for 4-element array.

Frequency (GHz)	Measured output power (dBm)	Ideal output (dBm)	Difference between desired and measured power (dB)
29.50	-28.90	-23.71	5.19
29.75	-32.60	-27.91	4.69
30.00	-38.00	-33.05	4.95

The difference was about 5 dB for all three measured cases. We are currently investigating the reason for this discrepancy. A preliminary investigation showed that it could be explained by the contribution of many factors, including scattering at the surface of the array, poorer spatial power combining antenna gain due to reduced ground plane size, and unequal phase and magnitude from the different unit cells due to slightly different size of the absorbing pieces.

3.6. Conclusions [1]

The design of a 37-element reflective spatial power combiner was presented. A passive version of the combiner was built and measured. An active 4-element prototype array was built and measured as a proof of concept.

3.6.1. Discussion

The possibility of using higher output power MMIC amplifiers was considered. It was found that the area of the MMIC chip was increasing faster than the output power provided by the chip. Consequently, it was not possible to include an amplifier with a larger area than the one already in use because of real estate limitations. Furthermore, higher output power chips might require a more complex heat sinking mechanism that would not fit in the actual unit cell. Finally, one of the advantages of using a relatively larger number of amplifiers in the actual configuration was the capability to provide an efficient phase profile for the active subreflector, which would not have been possible if a small number of unit cells were used.

3.6.2. Future work

In the actual unit cell, the use of absorbing material was necessary to increase the isolation and therefore suppress any undesired oscillation of the amplifier. However, this was not an efficient solution as it increased the path loss and therefore decreased the system gain of the spatial power combiner. It was also a non-practical solution as it increased the complexity of the unit cell. Therefore, the isolation must be increased using other means.

The major contributor to the isolation was the patch antenna. The current unit cell used the same patch for both receiving and transmitting, which was practical in terms of architecture as it reduced the real estate, but inefficient in terms of isolation. However, the isolation could potentially be increased to an acceptable level simply by using two patch antennas in the unit cell rather than a single one. The current single patch antenna is quite small with respect to the unit cell, i.e. 3.05 mm by 3.05 mm in a cell of 10 mm by 10 mm. By slightly reorganising the components in the unit cell, two patches with orthogonal polarisation could fit in the unit cell.

The last major problem relates to the DC biasing. The cavity allowed all the RF components to be electro-magnetically sealed, however this created assembly problems for the biasing. Unlike the rest of the unit cell, the DC biasing was not modular. Therefore, a modular DC biasing should also be employed, which would require a few minor modifications to the actual configuration.

Another option is to switch to a non-modular approach. With such an approach, the DC biasing could be done more easily, possibly with printed traces. In order to fix the real-estate problems, the DC traces could be embedded between two dielectric layers in such a way not to interfere with RF microstrip lines and/or printed patch antennas. For easier fabrication, the cavities could be removed; however this may increase the coupling between adjacent elements. Also, if the cavities are removed, the capacitors would require to be mounted horizontally, which may require rearranging each unit cell in order to make room for the capacitors.

41

<This page intentionally left blank>

42

4. Transmissive Tray

This chapter presents the preliminary development of the transmissive tray. Most of the work done at this point covers the development of the radiating element, however some comments will be made about the future design of the array.

4.1. Single Element

The particularity of the tray architecture with broadside elements is that, unlike conventional arrays or spatial power combining tiles, the feed network is perpendicular to the radiating element, as shown in Figure 25.

Many different approaches were considered, including perpendicular transition from microstrip to coplanar waveguide, probe-fed patch, direct feeding through a slot and proximity feed. At this point of the design, it was decided to minimise complex fabrication procedure, like those requiring soldering for example. This was the case of the coplanar waveguide feed and the probe feed. Directly feeding the patch can also be achieved, but it was shown that this method has the disadvantage of requiring a direct connection between the feed line and the slot [22]. The proximity feed, shown in Figure 26, is similar to the direct feed; however, the line is bent, which allows better tuning. Therefore, it was decided to use such a way to feed the patch.

4.1.1. Design

The patch antenna was fabricated on a rigid substrate in order to ensure the flatness of the substrate. For the transmission line, a high dielectric constant was chosen in order to make the feed lines thin. Table VIII presents the properties of the materials used.

A two-dimensional representation of the proximity-fed patch is shown in Figure 27. In this figure, the patch, the slot, the feed line, the ground plane clearance and the substrates are represented. The dimensions are given in Table IX. In order to obtain a good return loss, the length of the transmission line, i.e. the stub, had to be adjusted. The size of the ground plane clearance on the feed substrate was found to have an impact on the back lobe radiation. The structure was simulated in IMST Empire [23], including the metal jig, as shown in Figure 28. Photographs of the structure are shown in Figure 29.
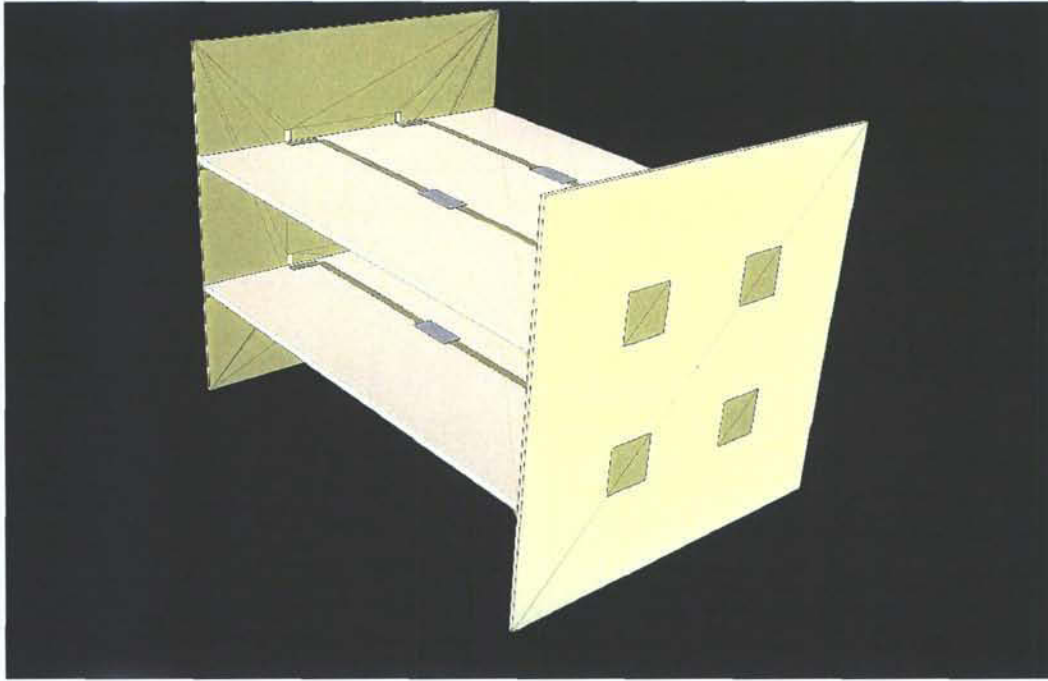
Figure 25: Three-dimensional representation of a 2 × 2 tray structure, showing the perpendicular substrates.
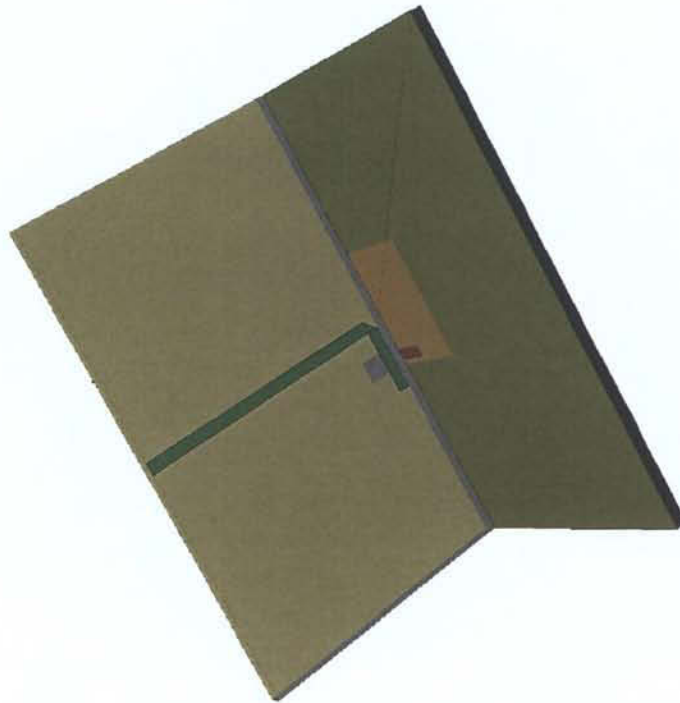

Figure 26: Three-dimensional representation of proximity coupling, showing perpendicular substrates, slots in the feed and patch ground planes and bent microstrip line.

44

Table VIII: Material description for the proximity-fed patch antenna.

	Patch substrate	Circuit substrate
Name	Rogers RO4003	Rogers TMM10i
Thickness	8 mils (0.2032 mm)	15 mils (0.381 mm)
Dielectric constant	3.38	9.80
Loss tangent	0.0027	0.0020

4.1.2. Simulation Results

Figure 30 presents the simulated S-parameter results for the proximity-fed patch antenna. The resonant frequency was 30.45 GHz for which the return loss was almost 35 dB. The radiation patterns simulated at 30.5 GHz are shown in Figure 31.

4.1.3. Measurement Results

Figure 32 presents the measured S-parameter results for the proximity-fed patch antenna. These results were different compared to the simulated results and many resonances were present. Among these resonances, there was one resonance around 30.5 GHz, which may coincide with the expected resonance frequency. The difference in return loss may be explained by the fact that there was a gap at the junction of the two perpendicular substrate boards, at the location of the proximity coupling.

The radiation patterns measured at 30.5 GHz are shown in Figure 33. There is a good agreement in the pattern shapes between the measured and simulated results. The gain was slightly less for the measured case, but only by a few decibels, which is commonly observed. The ripples in the measurement results may have been caused by the tower of the rotating table.

4.2. Future Work

The next step in the design of the tray spatial power combiner would be to study the design of an array. Essentially, the study would be the same as what was reported in section 3.2 for the tile architecture, i.e. the design would be similar to the design of the dual-fed patch antenna in the reflective approach. The major differences would be as follows:

- The array configuration would have to be square rather than an arbitrary shape. For instance, a 6 × 6 array should be the best candidate in this case;
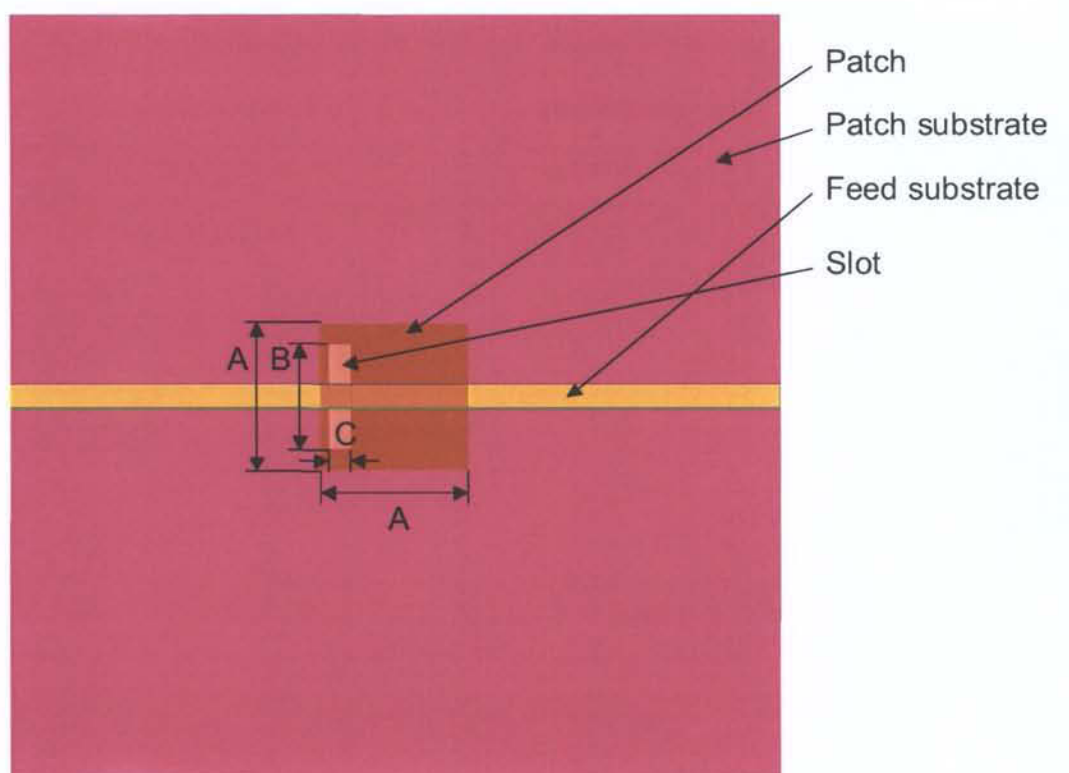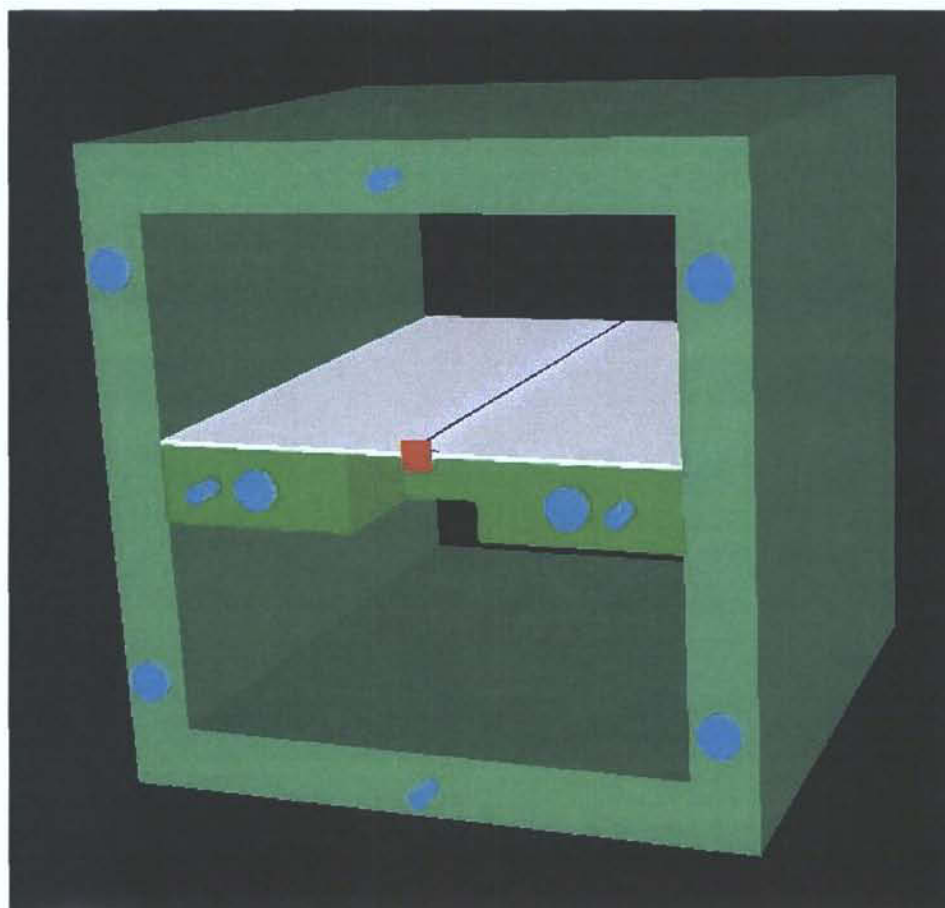
(a)
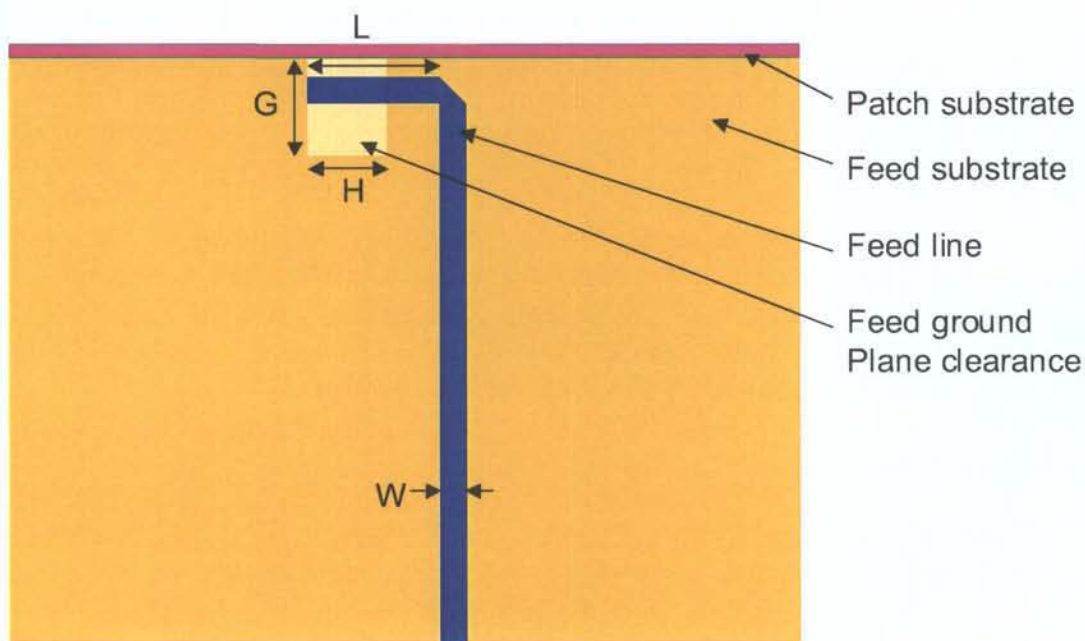
(b)

Figure 27: Two-dimensional representation of the proximity-fed patch antenna (a) front view; (b) top view.
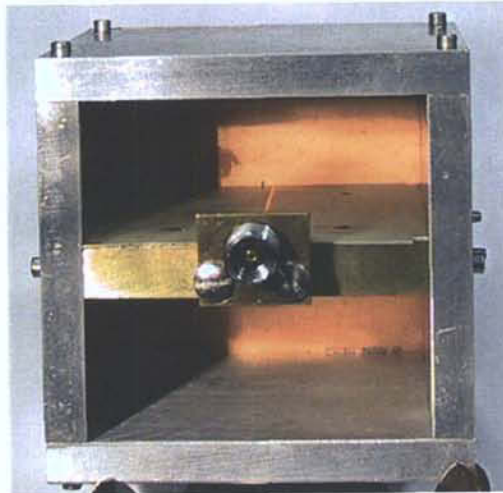
Table IX: Dimensions of the proximity-fed patch antenna.

Description	Symbol	Value (mm)
Patch size	A	2.3
Slot width	B	1.65
Slot height	C	0.35
Clearance width	G	1.495
Clearance length	H	1.2
Microstrip line width	W	0.4
Arm length	L	2.0

Figure 28: Three-dimensional representation of the proximity-fed patch antenna (patch substrate and ground plane are not shown).
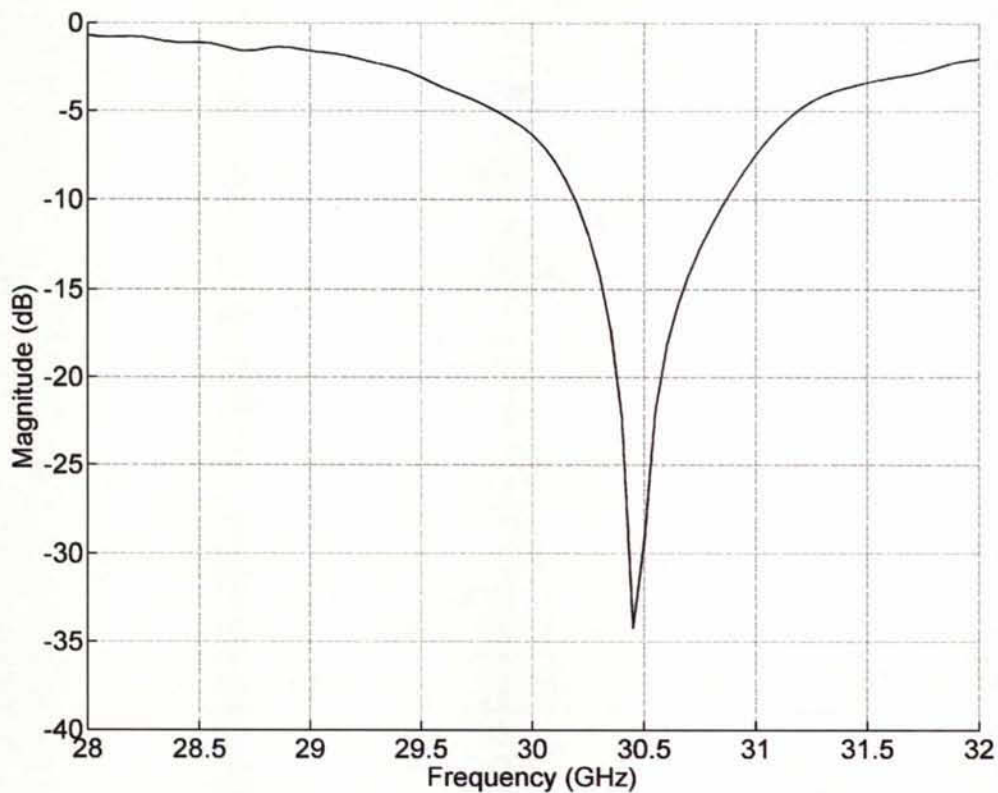
47
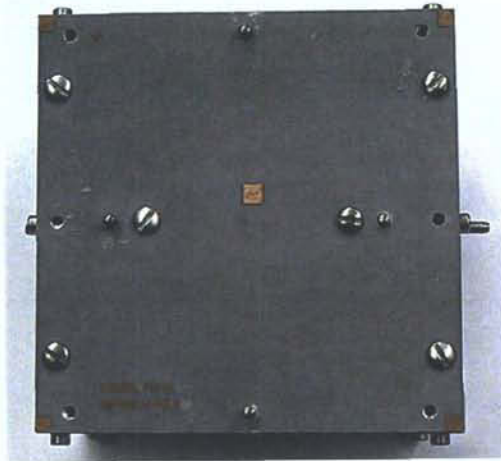
(a)

(b)

Figure 29: Photographs of the proximity-fed patch antenna; (a) front view,
(b) back view

Figure 30: Simulated S-parameters of the proximity-fed patch antenna.

- The unit cell size can be reduced down to about 0.7 wavelength, which would change the beam properties and require a different phase and amplitude profile. The achieved beam width would then be larger compared to a case where the unit cell size is 1 wavelength.

- The radiating element, i.e. the patch antenna, would be made of different substrate, would not be the same size, and would be fed differently. Therefore, this would change the radiation properties.
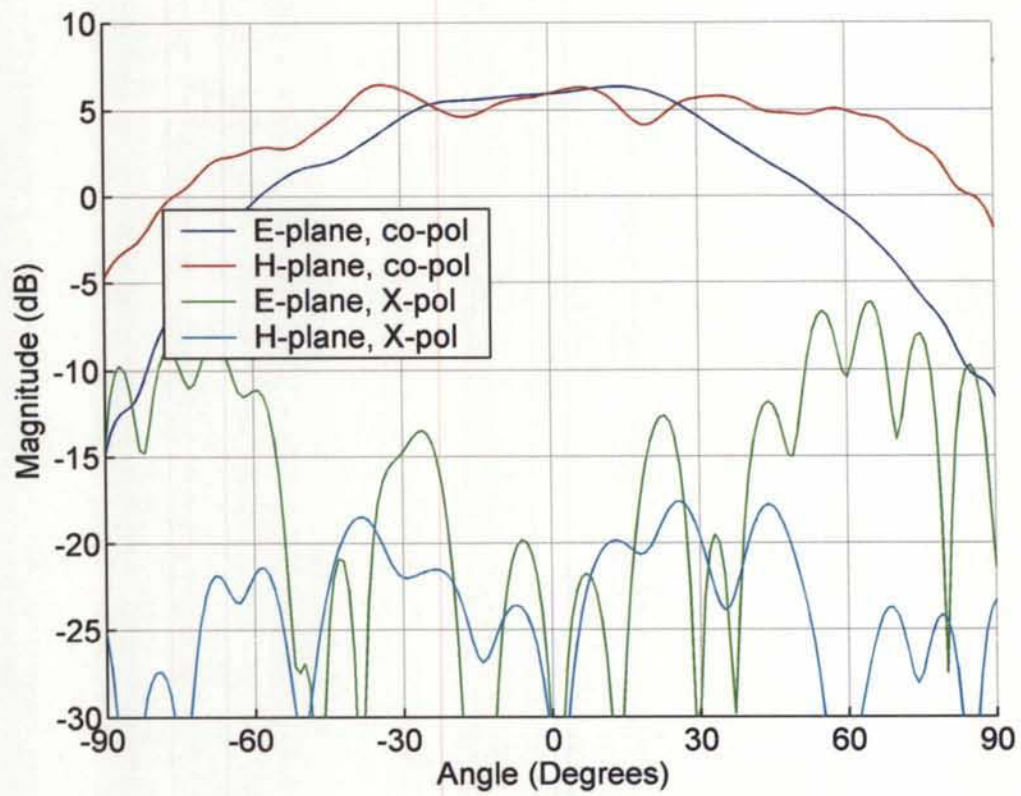
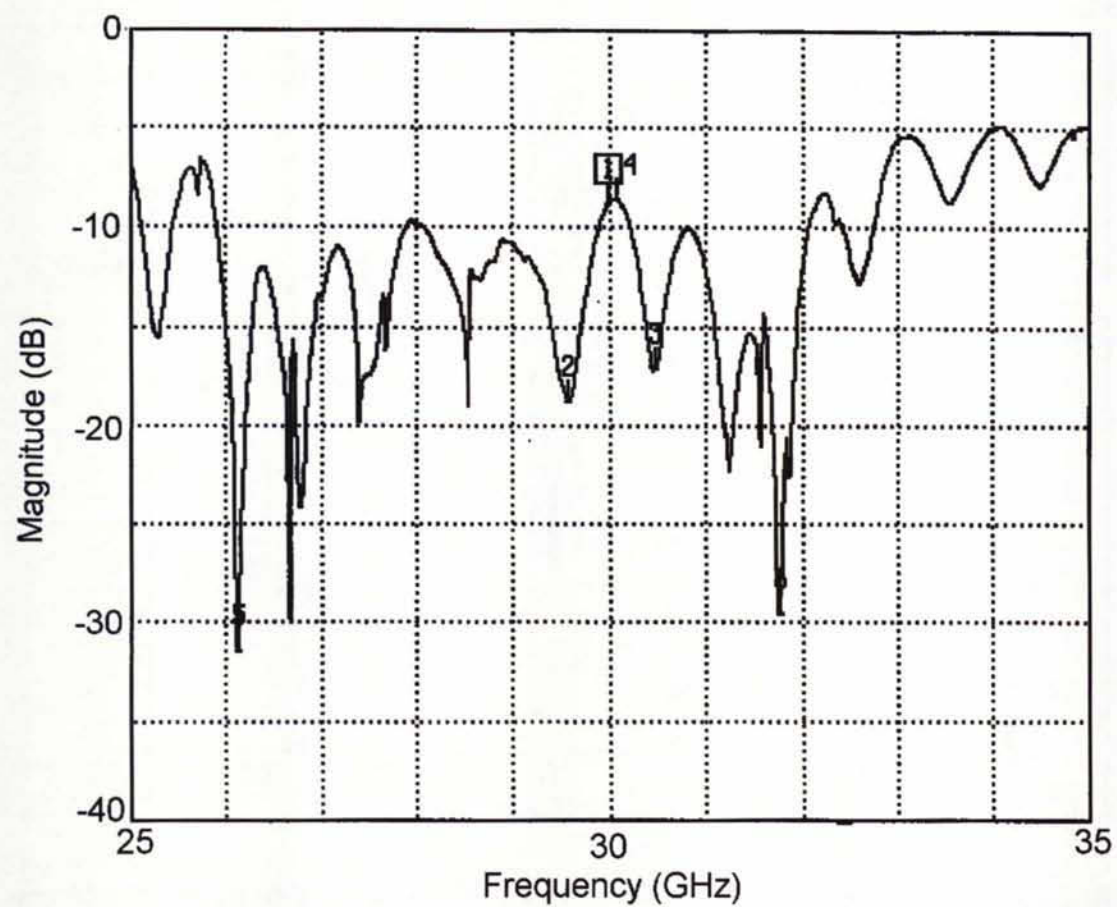**Figure 31: Simulated radiation patterns of the proximity-fed patch antenna.**

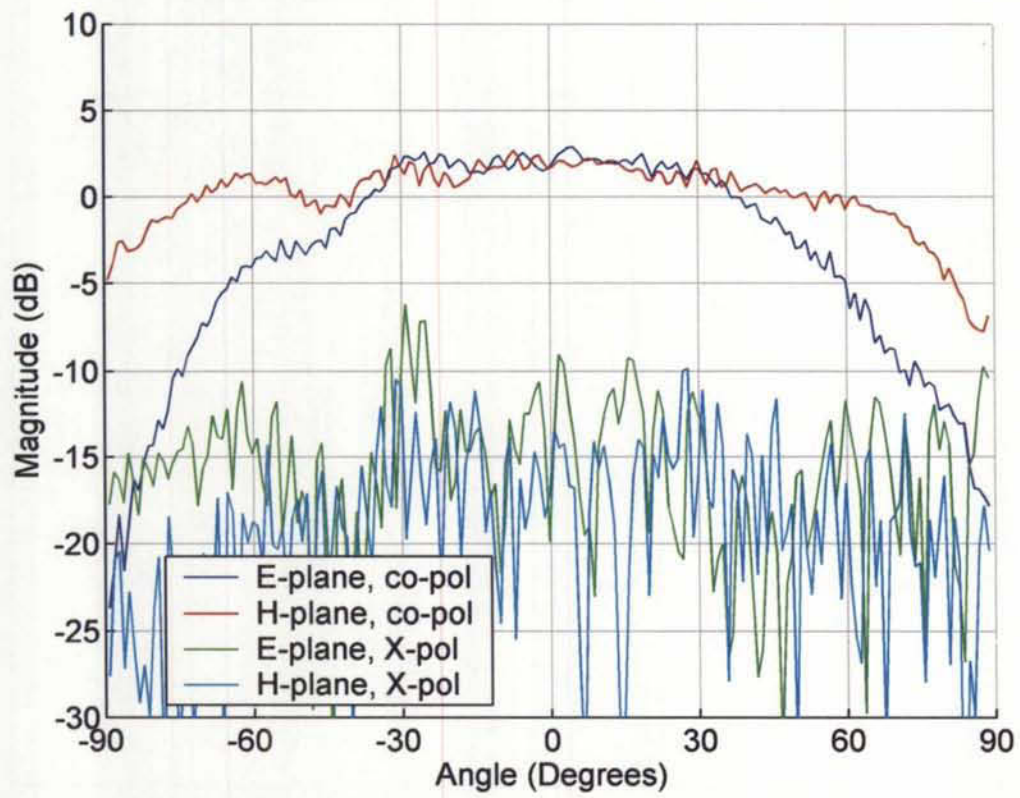Figure 32: Measured S-parameters of the proximity-fed patch antenna.

Figure 33: Measured radiation patterns of the proximity-fed patch antenna.

5. Conclusion

5.1. Summary

Phase 1 of the design of spatial power combining structures for feeding a reflectarray was reported. Two approaches were considered: a multilayer reflective tile and a transmissive tray. The single element for the multilayer reflective tile was fabricated and measured. The performances were similar to the predicted simulation results. A passive array has been fabricated and measured. Again, the performances were as expected. A single element for the transmissive tray was also fabricated and measured. A slight degradation was observed in the performance of the single-element antenna, which was found to be caused by a gap at the junction of the two substrate boards.

5.2. Future work

Phase 2 would allow for the completion of the spatial power combining design. The remaining tasks to be performed are listed below for the two different approaches.

For the reflective tile approach, the remaining tasks are:

- Redesigning the unit cell to allow for higher isolation between the input and output of the amplifier in order to avoid device oscillation; this implies using two microstrip patch antennas instead of a single dual-port antenna;

- Moving to a non-modular approach in order to reduce assembly problems related to the DC biasing, or implementing a modular DC biasing;

- Building a 37-element array and perform full measurements (beam shape, output power measurement, etc.).

For more details, refer to subsection 3.6.2.

For the transmissive tray approach, the remaining tasks are:

- Investigating if the current mechanical problems (i.e. gap between perpendicular substrate) allow for satisfying results and, if not, find solutions to improve the performance (e.g. soldering);

- Performing the electromagnetic design of an array to feed a main reflector; the array would probably be a square array composed of 36 elements (i.e. six trays, each containing six antennas);

- Performing the mechanical design of the array, including heat extraction means;

- Building and measuring the full array.

For more details, refer to subsection 4.2.

In addition to the above mentioned tasks, the main reflectarray would also need to be designed. This is not part of the spatial power combining project, however it is part of the high output power antenna at Ka band project.

Ultimately, the main reflectarray would be used for both transmission and reception. This implies offset feed in both cases. The reception part of the design has not been addressed and requires a significant amount of work; however it is not as challenging as the transmission part.

Work on Phase 2 of this project has not yet been approved, and will depend on upcoming priorities and available funding.

References

[1]   N. Gagnon, A. Petosa and J. Bradley, "A Ka-Band 37-Element Reflective Spatial Power Combiner," in *Proc. 11th Symp. Antenna Tech. App. Electromagn. (ANTEM)*, Saint-Malo, France, pp. 238-239, June 2005.

[2]   M. P. DeLisio and R. A. York, "Quasi-Optical and Spatial Power Combining," *IEEE Trans. Microwave Theory Tech.*, vol. 50, no. 3, pp. 929-936, March 2002.

[3]   M. A. Gouker, "Spatial Power Combining", Chapter 2 in *Active and Quasi-Optical Arrays for Solid-State Power Combining*, R. A. York and Z. B. Popović, Eds., Wiley, New York, 1997.

[4]   M. Gouker, "Toward Standard Figures-of-Merit for Spatial and Quasi-Optical Power-Combined Arrays," *IEEE Trans. Microwave Theory Tech.*, vol. 43, no. 7, pp. 1614-1617, July 1995.

[5]   B. Deckman, D. S. Deakin Jr., E. Sovero and D. Rutledge, "A 5-Watt, 37-GHz Monolithic Grid Amplifier," in *IEEE MTT-S Int. Microwave Symp. Dig.*, June 2000, pp. 805-808.

[6]   C.-T. Cheung, J. B. Hacker, G. Nagy and D. B. Rutledge, "A Waveguide Mode-Converter Feed for a 5-W, 34-Ghz Grid Amplifier," in *IEEE MTT-S Int. Microwave Symp. Dig.*, June 2002, pp. 1523-1526.

[7]   S. Ortiz, J. Hubert, L. Mirth, E. Schlecht and A. Mortazawi, "A 25 Watt and 50 Watt Ka-Band Quasi-Optical Amplifier," in *IEEE MTT-S Int. Microwave Symp. Dig.*, June 2000, pp. 797-800.

[8]   S. C. Ortiz, J. Hubert, L. Mirth, E. Schlecht and A. Mortazawi, "A High-Power *Ka*-Band Quasi-Optical Amplifier Array," *IEEE Trans. Microwave Theory Tech.*, vol. 50, no. 2, pp. 487-494, February 2002.

[9]   S. Ortiz, A. Al-Zayed and A. Mortazawi, "A Ka-Band Perpendicularly-Fed Patch Array for Spatial Power Combining," in *IEEE MTT-S Int. Microwave Symp. Dig.*, June 2002, pp. 1519-1522.

[10] X. Jiang, L. Liu, S. C. Ortiz, R. Bashirullah and A. Mortazawi, "A Ka-Band Power Amplifier Based on a Low-Profile Slotted-Waveguide Power-Combining/Dividing Circuit," *IEEE Trans. Microwave Theory Tech.*, vol. 51, no. 1, pp. 144-147, January 2003.

[11] J. Harvey, E. R. Brown, D. B. Rutledge and R. A. York, "Spatial Power Combining for High-Power Transmitters," *IEEE Microwave Mag.*, vol. 1, no. 4, pp. 48-59, December 2000.

[12] Z. Popovic, "T/R Lens Amplifier Antenna Arrays for X-band and Ka-band," *App. Microwave Wireless*, vol. 11, no. 2, pp. 30-45, February 1999.

[13] A. J. Zaman and R. Q. Lee, "A Spherical to Plane Wave Transformation Using a Reflectarray," in *IEEE AP-S Int. Symp. Dig.*, July 1997, pp. 1284-1287.

[14] H. J. Song and M. E. Bialkowski, "Spatial Power Combiner Using an Active Reflectarray of Dual-Feed Aperture Coupled Microstrip Patch Antennas," in *IEEE AP-S Int. Symp. Dig.*, July 2001, pp. 768-771.

[15] M. E. Bialkowski and H. J. Song, "Investigations Into a Power-Combining Structure Using a Reflect Array of Dual-Feed Aperture-Coupled Microstrip Patch Antennas," *IEEE Trans. Antennas Propagat.*, vol. 50, no. 6, pp. 841-849, June 2002.

[16] J. Shaker, N. Gagnon and M. Cuhaci, "A Novel Quasioptical Amplifier," *Microwave and Optical Technology Letters*, vol. 24, no. 2, pp. 93-99, January 2000.

[17] N.-S. Cheng, P. Jia, D. B. Rensch and R. A. York, "A 120-W *X*-Band Spatially Combined Solid-State Amplifier," *IEEE Trans. Microwave Theory Tech.*, vol. 47, no. 12, pp. 2557-2561, December 1999.

[18] Ansoft, *Ensemble 8.0 - Getting Started*, Pittsburgh, February 2001.

[19] Mathsoft, *Mathcad 2001 Professional User's Guide with Reference Manual*, Cambridge, MA, November 2000.

[20] Y. Lee, K. W. Brown and A. Prata Jr., *RASCAL Version 2.1 - Interactive Reflector Antenna Synthesis & Analysis Software User's Manual*, Los Angeles, 1995.

[21] Far Field, *ARPS, Antenna Radiation Pattern Software - User's Guide*, Ottawa, Canada, 1998.

[22] K. W. Leung and M. W. To, "Slot-coupled dielectric resonator antenna using a proximity feed on a perpendicular substrate," *Electronics Letters*, vol. 33, no. 20, pp. 1665-1666, September 1997.

[23] IMST GmbH, *User and Reference Manual for the 3D-EM Time Domain Simulator Empire*, Kamp-Lintfort, Germany, 2002.
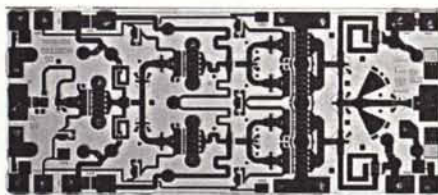
Appendix A: TriQuint TGA4509-EPU Specification Sheet

TriQuint 🔷
SEMICONDUCTOR.

27 - 32 GHz 1W Power Amplifier   TGA4509-EPU

Chip Dimensions 2.4 mm x 1.2 mm x 0.1 mm

Key Features
- 22 dB Nominal Gain @ 30 GHz
- 30 dBm Nominal Pout @ P1dB
- 25% PAE @ P1dB
- -10 dB Nominal Return Loss
- Built-in Power Detector
- 0.25-µm mmW pHEMT 3MI
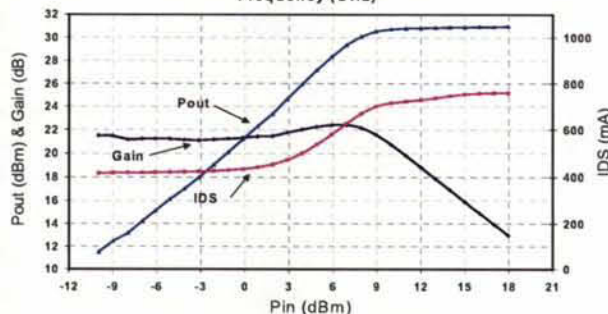- Bias Conditions: Vd = 4 - 6 V, Idq = 420 mA

Primary Applications
- Point to Point Radio
- Point to Multi-point Radio
- LMDS
- Satellite Ground Terminal

Fixtured Measured Performance

Bias Conditions: Vd = 6 V, Id =420 mA
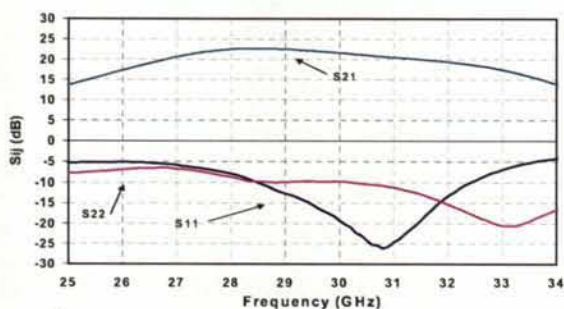
Data taken
@ 30 GHz

Note: Devices designated as EPU are typically early in their characterization process prior to finalizing all electrical and process specifications. Specifications are subject to change without notice.

Advance Product Information
January 23, 2003
TGA4509-EPU

TABLE I

MAXIMUM RATINGS 1/

Symbol	Parameter	Value	Notes
V$^+$	Positive Supply Voltage	7 V	
V$^-$	Negative Supply Voltage Range	-5 V to 0 V	
|Ig|	Gate Current	35.2 mA	
I$^+$	Positive Supply Current	930 mA	2/, 5/
P$_D$	Power Dissipation	TBD	
P$_{IN}$	Input Continuous Wave Power	22 dBm	
T$_{CH}$	Operating Channel Temperature	150 °C	3/, 4/
T$_M$	Mounting Temperature (30 seconds)	320 °C	
T$_{STG}$	Storage Temperature	-65 °C to 150 °C	

1/ These values represent the maximum operable values of this device
2/ Total current for the entire MMIC
3/ These ratings apply to each individual FET
4/ Junction operating temperature will directly affect the device mean time to failure (MTTF). For maximum life it is recommended that junction temperatures be maintained at the lowest possible levels.
5/ The maximum supply current from one side is 650 mA. From both sides, the maximum supply current is 930 mA.

TABLE II

ELECTRICAL CHARACTERISTICS

(T$_A$ = 25°C, Nominal)

Parameter	Units	Typical
Drain Operating Voltage	V	6
Quiescent Current	mA	420
Small Signal Gain @ 30 GHz	dB	22
Gain Flatness	dB/50MHz	0.0660
Input Return Loss (Linear Small Signal)	dB	-10
Output Return Loss (Linear Small Signal)	dB	-10
Reverse Isolation	dB	-40
CW Output Power @ P1dB	dBm	30
Power Added Efficiency @ P1dB	%	25
P1dB temperature coeff. TC (-40 to +85 °C)	dB/deg C	0.0135
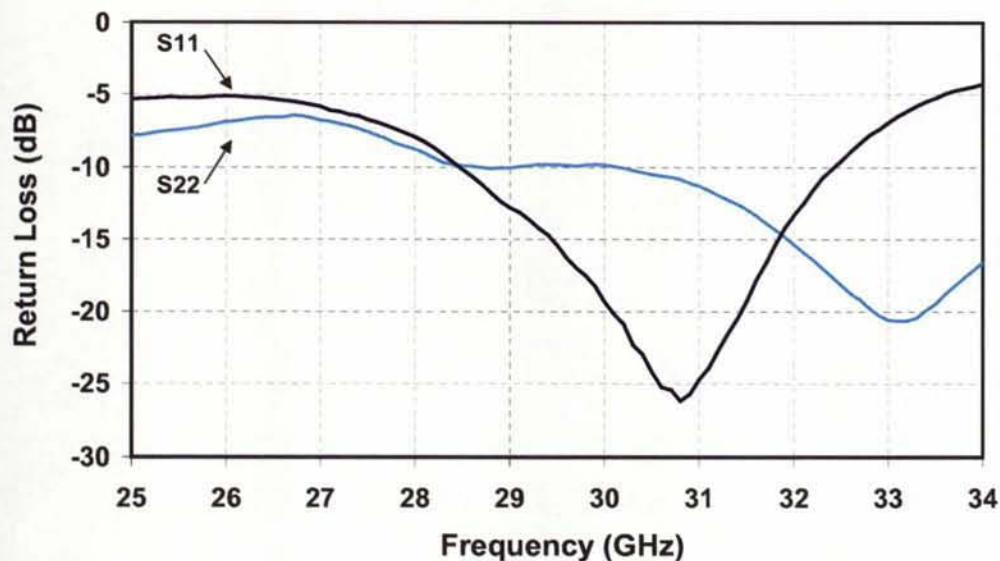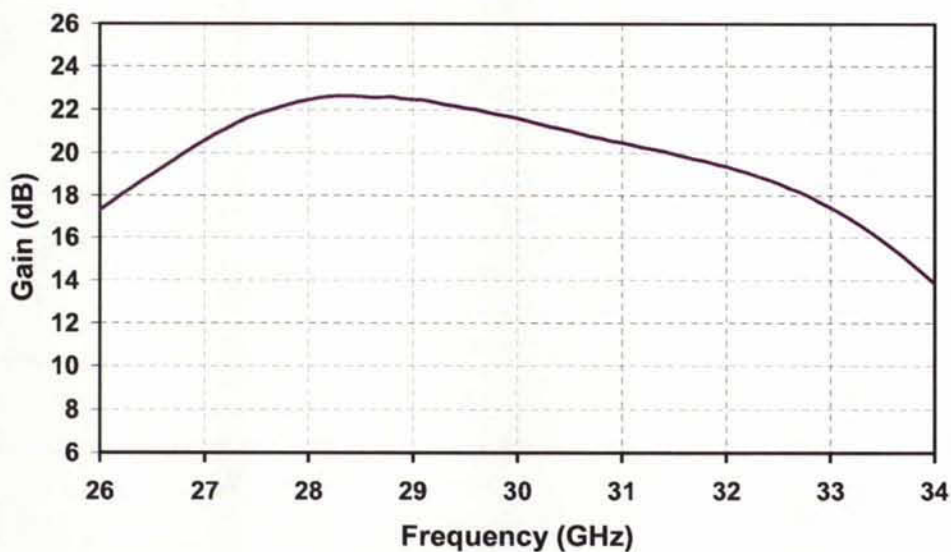
Measured Fixtured Data

Bias Conditions: Vd = 6 V, Id = 420 mA

Note: Devices designated as EPU are typically early in their characterization process prior to finalizing all electrical and process specifications. Specifications are subject to change without notice.
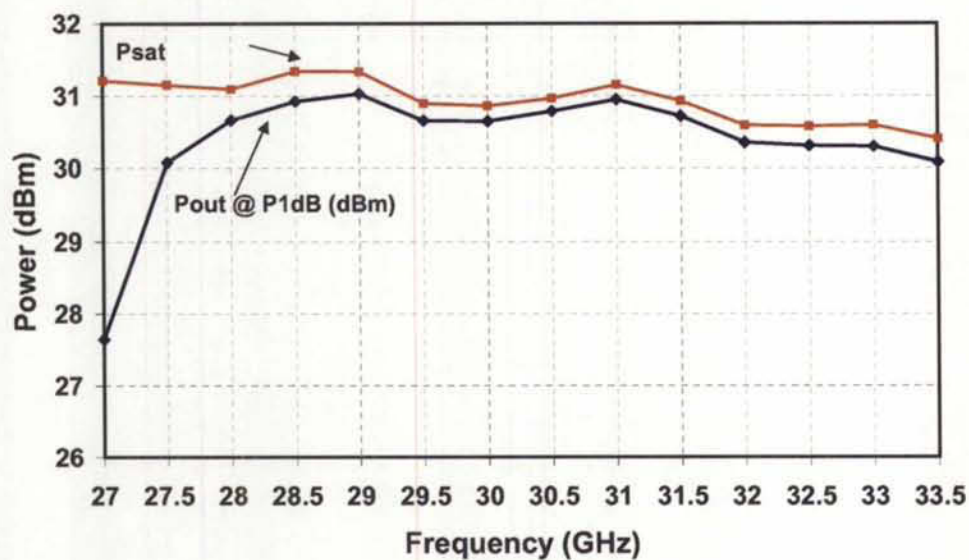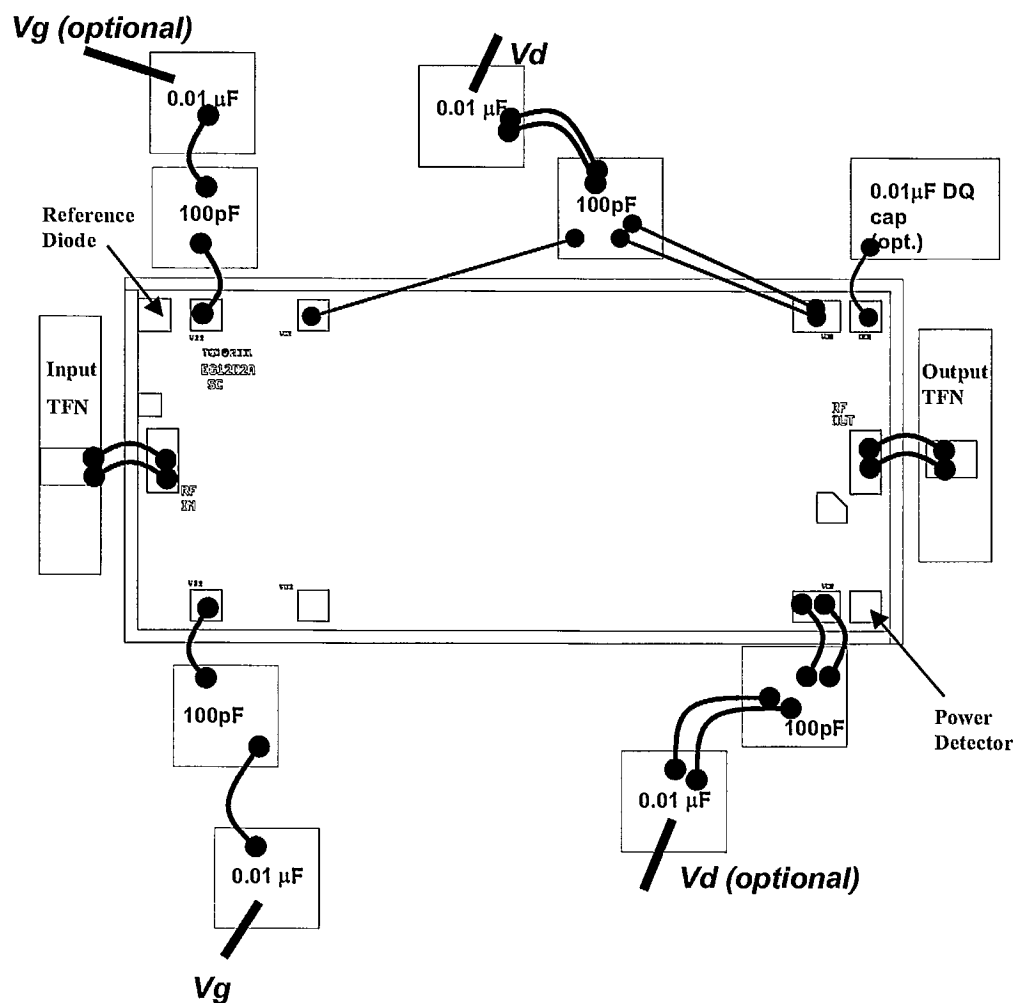
TriQuint
SEMICONDUCTOR.

Measured Fixtured Data

Bias Conditions: Vd = 6 V, Id = 420 mA

4

Recommended Assembly Diagram

Notes:
1. Connection to power det, ref diode shown.
2. 1 µF cap on gate & drain power supplies lines is required.
3. Gate voltage can either be from one side or both sides.
4. Drain voltage is required from both sides for Id > 650 mA.

GaAs MMIC devices are susceptible to damage from Electrostatic Discharge. Proper precautions should be observed during handling, assembly and test.

Note: Devices designated as EPU are typically early in their characterization process prior to finalizing all electrical and process specifications. Specifications are subject to change without notice.

On-chip diode functions as envelope detector
External coupler and DC bias required

TGA4509 measured detector voltage offset vs output power with 20dB
coupler: Vb=0.8V, f = 30GHz, Coupler loss is uncalibrated, 10KΩ load
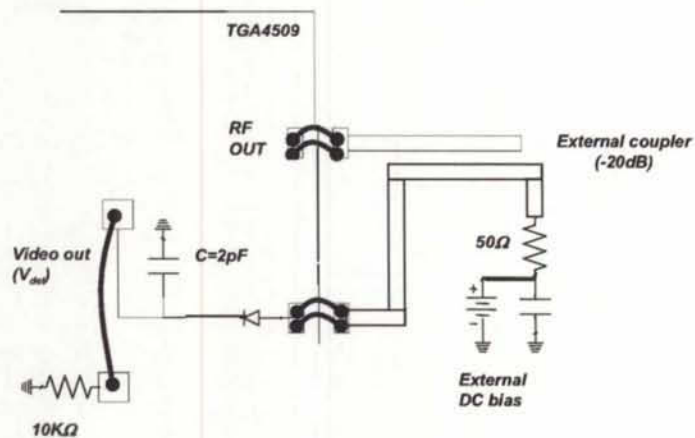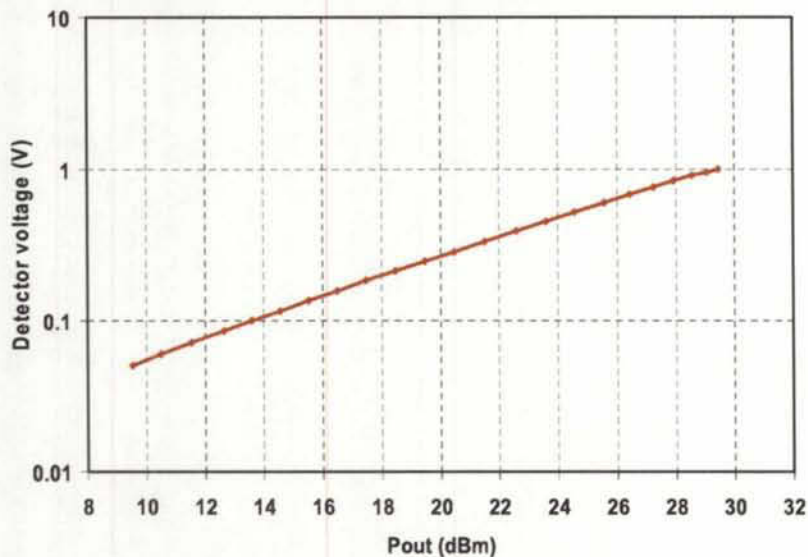
Note: Devices designated as EPU are typically early in their characterization process prior to finalizing all electrical and process specifications. Specifications are subject to change without notice.
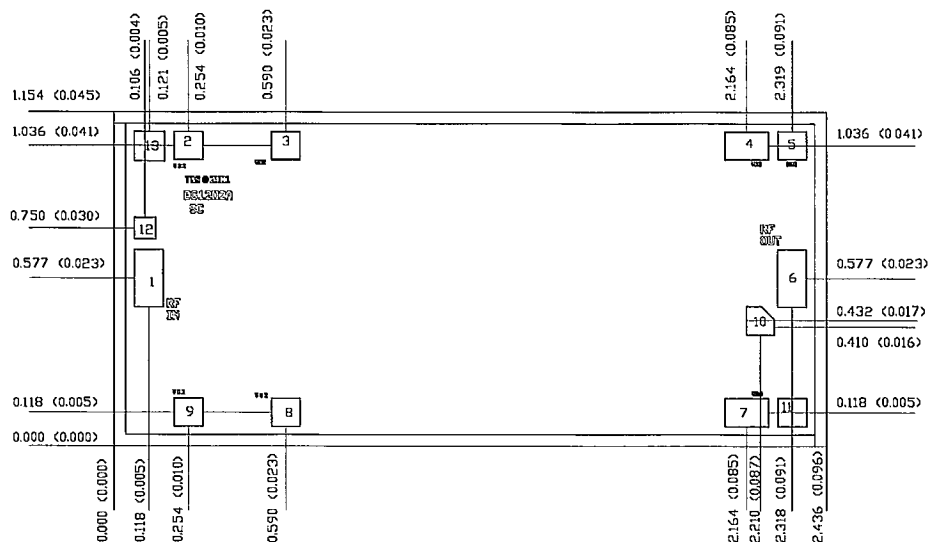
Mechanical Drawing

Units: millimeters (inches)
Thickness: 0.100 (0.004)
Chip edge to bond pad dimensions are shown to center of bond pad
Chip size tolerance: +/- 0.051 (0.002)

GND IS BACKSIDE OF MMIC

Bond Pad #1 (RF Input)	0.098 × 0.198 (0.004 × 0.008)
Bond Pad #2 (VG1)	0.098 × 0.098 (0.004 × 0.004)
Bond Pad #3 (VD1)	0.098 × 0.098 (0.004 × 0.004)
Bond Pad #4 (VD1)	0.148 × 0.098 (0.006 × 0.004)
Bond Pad #5 (DEQ)	0.098 × 0.098 (0.004 × 0.004)
Bond Pad #6 (RF Output)	0.098 × 0.198 (0.004 × 0.008)
Bond Pad #7 (VD2)	0.148 × 0.098 (0.006 × 0.004)
Bond Pad #8 (VD2) Optional	0.098 × 0.098 (0.004 × 0.004)
Bond Pad #9 (VG2) Optional	0.098 × 0.098 (0.004 × 0.004)
Bond Pad #10 (PWR DET)	0.095 × 0.096 (0.004 × 0.004)
Bond Pad #11 (PWR DET)	0.098 × 0.098 (0.004 × 0.004)
Bond Pad #12 (REF Diode)	0.071 × 0.071 (0.003 × 0.003)
Bond Pad #13 (REF Diode)	0.102 × 0.102 (0.004 × 0.004)

GaAs MMIC devices are susceptible to damage from Electrostatic Discharge. Proper precautions should be observed during handling, assembly and test.

Note: Devices designated as EPU are typically early in their characterization process prior to finalizing all electrical and process specifications. Specifications are subject to change without notice.

Assembly Process Notes

Reflow process assembly notes:

- Use AuSn (80/20) solder with limited exposure to temperatures at or above 300 °C for 30 sec.
- An alloy station or conveyor furnace with reducing atmosphere should be used.
- No fluxes should be utilized.
- Coefficient of thermal expansion matching is critical for long-term reliability.
- Devices must be stored in a dry nitrogen atmosphere.

Component placement and adhesive attachment assembly notes:

- Vacuum pencils and/or vacuum collets are the preferred method of pick up.
- Air bridges must be avoided during placement.
- The force impact is critical during auto placement.
- Organic attachment can be used in low-power applications.
- Curing should be done in a convection oven; proper exhaust is a safety concern.
- Microwave or radiant curing should not be used because of differential heating.
- Coefficient of thermal expansion matching is critical.

Interconnect process assembly notes:

- Thermosonic ball bonding is the preferred interconnect technique.
- Force, time, and ultrasonics are critical parameters.
- Aluminum wire should not be used.
- Discrete FET devices with small pad sizes should be bonded with 0.0007-inch wire.
- Maximum stage temperature is 200 °C.

GaAs MMIC devices are susceptible to damage from Electrostatic Discharge. Proper precautions should be observed during handling, assembly and test.

Note: Devices designated as EPU are typically early in their characterization process prior to finalizing all electrical and process specifications. Specifications are subject to change without notice.

TriQuint Semiconductor Texas: Phone (972)994-8465 Fax (972)994 8504 Web: www.triquint.com (8)